



UNIVERSIDAD  
POLITECNICA  
DE VALENCIA



Máster Universitario  
en Tecnologías, Sistemas y  
Redes de Comunicaciones

# Síntesis de Líneas de Transmisión Metamateriales con Mapeado Espacial Agresivo

*Autor:* Ana María Rodríguez Pérez

*Director:* Vicente E. Boria Esbert

*Fecha de comienzo:* 6/04/2010

*Lugar de trabajo:* Grupo de Aplicaciones de Microondas del iTEAM



*Objetivos —*

Muchos de los dispositivos y componentes pasivos que se utilizan en los terminales de comunicaciones se basan en líneas de transmisión, y sus dimensiones pueden resultar demasiado grandes para determinadas aplicaciones y/o frecuencias de aplicación. En ocasiones, estas líneas de transmisión convencionales se pueden sustituir por líneas artificiales basadas en la inclusión de metamateriales, las cuales presentan un mayor número de grados de libertad para su diseño que las líneas tradicionales. Esta característica hace que se pueda reducir el tamaño del dispositivo, pero se consigue a costa de añadir una mayor complejidad al proceso de diseño.

Con este trabajo se propone aplicar técnicas basadas en Mapeado Espacial, en inglés “Space Mapping” (SM) para simplificar el proceso de síntesis de estructuras basadas en líneas de transmisión de metamateriales que en general es arduo y laborioso, con un alto coste tanto en términos de tiempo como de recursos humanos y materiales. Este proyecto podría ser de gran interés para aplicaciones aeronáuticas, aeroespaciales o de comunicaciones inalámbricas, donde el tamaño de los componentes es un factor crítico, al permitir reducir el tamaño de los dispositivos utilizados convencionalmente sin pérdida de prestaciones, y de ahí su claro interés práctico.

*Metodología —*

Toda estrategia basada en técnicas de SM asume que la estructura estudiada puede simularse usando dos modelos: uno denominado *fino* o en inglés *fine*, que es complejo, costoso computacionalmente aunque muy preciso, y otro *grueso/coarse* que es más rápido en términos de CPU pero también más inexacto. Por tanto, se ha de elegir un tipo de estructura de la cual conozcamos el circuito eléctrico equivalente (en nuestro caso modelo grueso/coarse), y que éste permita reproducir lo más fielmente posible su respuesta electromagnética (nuestro modelo fino). De lo bueno que sea este modelo grueso dependerá en gran medida el comportamiento de las técnicas basadas en SM, por tanto es una pieza clave a la hora de que la aplicación práctica del algoritmo tenga éxito.

Una vez elegida la celda unidad de diseño y previamente a la aplicación algoritmo, se necesita:

- Decidir qué parámetros de optimización pueden ser los más adecuados a utilizar en cada espacio de simulación.
- Distintas estrategias son factibles de implementar en ambos espacios: trabajar sobre mismo tipo de variables o no, número de parámetros idéntico o distinto, etc.
- Estimar el punto inicial en los modelos grueso y fino, y comprobar con el modelo fino que el resultado no esté demasiado alejado de la respuesta objetivo (para evitar problemas de convergencia).

Las técnicas basadas en SM consiguen una optimización eficiente del modelo fino (EM) mediante la optimización iterativa del modelo grueso (circuito equivalente). Se pretende llegar a las dimensiones de la estructura que reproduzcan lo más fielmente posible el comportamiento de la respuesta objetivo, haciendo el menor número de simulaciones EM.

Herramientas a utilizar en la realización del proyecto:

- Simulador electromagnético Ansoft Designer que tiene integrado modulo Nexxim que permite realizar simulaciones circuitales.
- MATLAB. Software que permitirá aparte de la realización de distintas instrucciones, realizar de forma automática llamada y manipulación a programas externos, en nuestro caso por ejemplo Ansoft Designer. Además consta de una toolbox de optimización (optimtool) que se utilizará por ejemplo para el cálculo del punto inicial del algoritmo.
- CSRR.exe herramienta que permite dadas unas dimensiones físicas CSRR y características del sustrato, calcular la frecuencia de resonancia y parámetros eléctricos que modelan al resonador.

*Resultados —*

Se ha conseguido el desarrollo de una herramienta eficiente y automática para la síntesis de un tipo de líneas de transmisión que exhiben una permitividad dieléctrica equivalente negativa. Estas son resultado de cargar con resonadores de anillos abiertos complementarios, más conocidos entre la comunidad científica

por sus siglas en inglés CSRR (Complementary Split Ring Resonators) sobre una línea microstrip (grabados en el plano de tierra de la línea). Se logra convergencia en pocas iteraciones con una excelente concordancia entre las respuestas final y objetivo.

*Líneas futuras —*

Este trabajo abre un camino prometedor para la aplicación de este tipo de metodología a otro tipo de diseños más complejos basados en líneas de metamateriales cuya síntesis es también ardua y laboriosa. Además se está empezando a estudiar otras estrategias y algoritmos complementarios que permitan hacer esta técnica más robusta y/o acelerar la convergencia.

*Publicaciones —*

**A. Rodríguez**, J. Selga, M. Gil, J. Carbonell, V. E. Boria, F. Martín “Automated Synthesis of Resonant-type Metamaterial Transmission Lines using Aggressive Space Mapping”. IEEE MTT International Microwave Symposium, May 2010.

J. Selga, **A. Rodríguez**, M. Gil, J. Carbonell, V. E. Boria and F. Martín, “Towards the automatic layout synthesis in resonant-type metamaterial transmission lines”. IET Microwave Antennas Propagation, Volume 4, Issue 8, p.1007–1015, August 2010.

J. Selga, **A. Rodríguez**, M. Gil, J. Carbonell, V. E. Boria, F. Martín "Synthesis of Planar Microwave Circuits through Aggressive Space Mapping using Commercially Available Software Packages". International Journal of RF and Microwave Computer-Aided Engineering. Volume 20, Issue 5, pages 527–534, September 2010.

*Abstract —*

A technique for the automated generation of the layout of microstrip lines loaded with complementary split ring resonators is proposed. This synthesis strategy presents a great practical interest, due to the reduction in terms of computational efforts, that is achieved without any significant lack of accuracy in the final solution. The application makes use of an aggressive space mapping (ASM) algorithm based on a constrained Broyden-based input approach. In this case, the parameter extraction (PE) does not require of any optimization, since the circuital parameters of the metamaterial transmission line can be determined following a straightforward method.

**ÍNDICE**

<b>I. Introducción .....</b>	<b>4</b>
I.1. Metamateriales.....	4
I.2. Líneas de Transmisión Metamateriales .....	6
I.2.1. Líneas cargadas CL. ....	7
I.2.2. Líneas de tipo resonante .....	8
<b>II. Mapeado Espacial .....</b>	<b>10</b>
II.1.Mapeado espacial agresivo .....	11
<b>III. Celda de Estudio .....</b>	<b>13</b>
III.1.Topología y Modelo Eléctrico Equivalente.....	13
III.2. Extracción de Parámetros.....	15
<b>IV. Automatización .....</b>	<b>16</b>
IV.1.Planteamiento .....	17
IV.2. Implementación del método.....	18
IV.2.1. Inicialización .....	18
IV.2.2. Diagrama de Flujo .....	22
IV.2.3. Estructura del Código .....	23
<b>V. Resultados .....</b>	<b>24</b>
IV.1.Ejemplo de validación.....	24
IV.2. Ejemplo de aplicación .....	25
<b>VI. Conclusiones .....</b>	<b>27</b>
<b>Agradecimientos .....</b>	<b>27</b>
<b>Referencias .....</b>	<b>28</b>
<b>Anexos .....</b>	<b>31</b>

## I. INTRODUCCIÓN

Desde la aparición de los primeros metamateriales, éstos han recibido una gran atención por parte de la comunidad científica debido a las interesantes propiedades que presentan y sus múltiples aplicaciones. El rango de operación de los metamateriales es muy amplio. En el ámbito de las microondas se usan principalmente para la miniaturización y mejora de prestaciones de diferentes dispositivos de telecomunicaciones, como son: filtros, divisores de potencia, antenas...

En este primer apartado se realiza una breve introducción a los metamateriales, pues es un campo aún novedoso y en continua evolución, apuntando sus características principales así como su aplicación en líneas de transmisión.

### I.1. METAMATERIALES

Aunque no existe una definición universalmente aceptada, se suelen considerar metamateriales a aquellas estructuras periódicas o quasi-periódicas que son fabricadas artificialmente, y presentan unas propiedades electromagnéticas controlables diferentes a las de sus elementos constituyentes, y en ocasiones, no existentes en la naturaleza. Las dimensiones o período de repetición de estas estructuras típicamente se considera mucho menor que la longitud de onda ( $\lambda$ ) a la frecuencia de interés. Las propiedades electromagnéticas, que definen la propagación del campo eléctrico y magnético de una onda en el medio, vienen determinadas por la permitividad dieléctrica ( $\epsilon$ ) y la permeabilidad magnética ( $\mu$ ) del medio. Existen cuatro posibles grupos de materiales en función de los signos que  $\epsilon$  y  $\mu$  puedan tener, ver Fig.1.

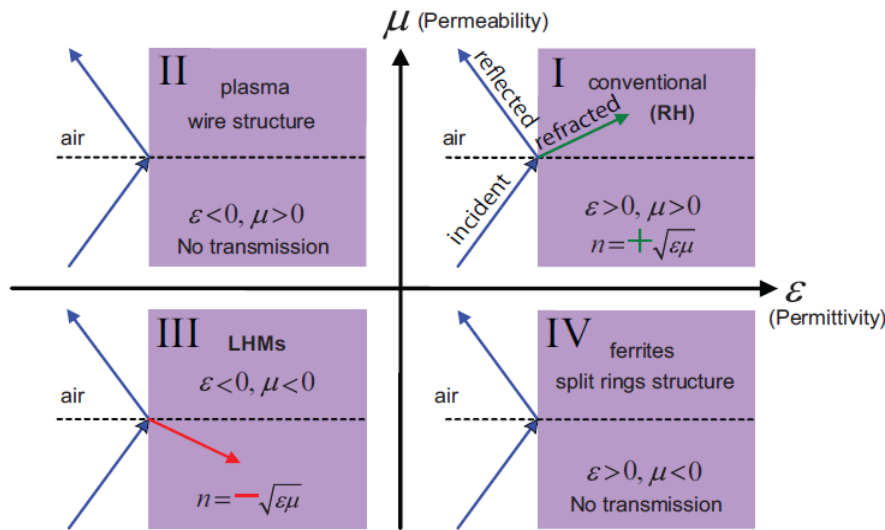


**Fig. 1.** Clasificación de los distintos materiales según el signo de  $\epsilon$  y  $\mu$ .

Los medios que presentan  $\epsilon$  y  $\mu$  con signos distintos, presentan valores imaginarios de la constante de propagación  $k$  y el índice de refracción  $n$ , y como consecuencia en ellos no puede existir propagación. Las ecuaciones que definen dichos parámetros se presentan a continuación

$$k^2 = \frac{\omega^2}{c^2} n^2 \quad (1)$$

donde  $\omega$  es la frecuencia angular,  $c$  la velocidad de propagación en el espacio libre y  $n$

$$n^2 = \epsilon\mu \quad (2)$$

Si presentan el mismo signo ( $\epsilon$  y  $\mu$ ), sí hay propagación al resultar  $k$  un numero real. Los materiales con ambos parámetros positivos situados en el primer cuadrante de la Fig.1 son los llamados materiales “right-handed” (RHM), que son los más habituales en la naturaleza y por tanto los más estudiados.

Por el contrario, los materiales que presentan al mismo tiempo  $\epsilon$  y  $\mu$  negativos, sólo habían sido estudiados de forma teórica por Veselago en 1968 [1], mientras que su implementación y verificación física no se logró hasta el año 2000 [2]. Dado que en la naturaleza no existen medios conocidos con permitividad y permeabilidad efectiva negativa simultáneamente, para obtener un medio con estas características hay que combinar dos medios que tengan dichas propiedades por separado en un mismo rango de frecuencias. Fueron Smith et al. [2] de la Universidad de California en San Diego los que realizan la primera estructura zurda (LHM, del inglés left-handed media), constituida por distribuciones periódicas de postes metálicos en combinación con una agrupación (array) en paralelo de resonadores de anillos abiertos (Split Ring Resonator, SRR), a una frecuencia aproximada de 12 GHz. Se puede observar de forma gráfica dicha estructura en la Fig. 2. El resonador SRR, introducido por Pendry et al. en 1999, fue la primera estructura resonante no magnética realizada capaz de proporcionar valores de permeabilidad efectiva negativa, y constituyó un gran avance en el estudio de los materiales [3].



**Fig. 2.** Primer medio zurdo realizado combinando periódicamente postes metálicos y resonadores SRR [2].

El nombre de materiales zurdos alude a la orientación de los vectores de onda  $\vec{k}$  y de Poynting  $\vec{S}$  que presentan la misma dirección, pero tienen sentidos opuestos, por lo que las velocidades de fase y de grupo son también antiparalelas.

$$\vec{S} = \vec{E} \times \vec{H} \quad (3)$$

El cambio simultáneo en el signo de  $\epsilon$  y  $\mu$  supone que la tupla de vectores representados en la Fig. 3, pase de tener orientación a derechas a tenerla a izquierdas.

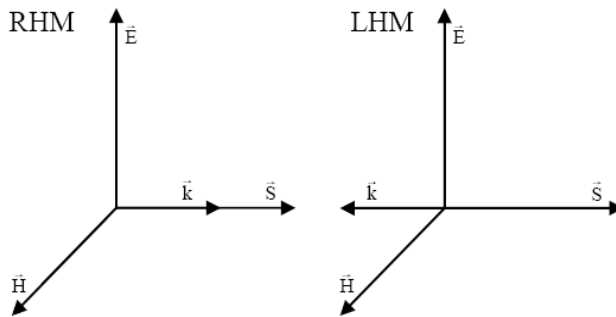


**Fig. 3.** Representación de los campos, vector de propagación y vector de Poynting en los medios diestros (RHM) y los zurdos (LHM)

Esto motiva distintos efectos físicos contrarios a los de los compuestos diestros más habituales RHM, con  $\epsilon$  y  $\mu$  positivos, como son: inversión del desplazamiento Doppler, inversión de la radiación de Cherenkov y cambios en las ecuaciones de Fresnel y en el principio de Fermate. Además, uno de los principios más básicos de la óptica como es la ley de Snell también sufre una inversión en la interfaz entre un medio left-handed y un medio right-handed. Así, las ondas electromagnéticas al atravesar dicha interfaz sufren una refracción negativa, ver Fig. 4.

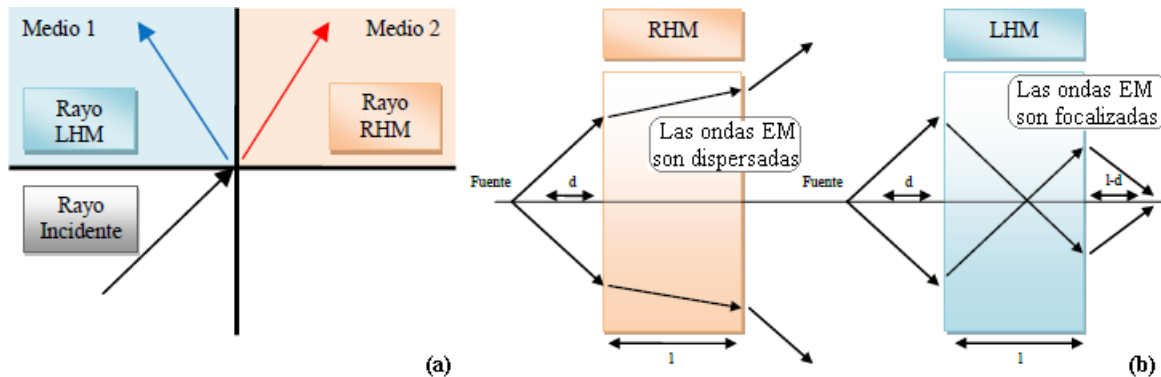


**Fig. 4.** Refracción para un medio diestro (RHM) y un medio zurdo (LHM) (a). Comportamiento de una onda que atraviesa una lente RHM y una lente LHM (b).

## I.2. LÍNEAS DE TRANSMISIÓN METAMATERIALES

Las líneas de transmisión basadas en metamateriales han sido ampliamente estudiadas en los últimos años, y gran parte del esfuerzo de investigación se ha centrado en su síntesis [4]. En contraste con las primeras estructuras LH que eran volumétricas y no compatibles con procesos tecnológicos planares, las líneas de transmisión metamateriales sí son compatibles, y presentan en general unas dimensiones menores a las de las líneas convencionales, y por tanto son consideradas más adecuadas para muchas aplicaciones prácticas. Presentan mayor flexibilidad de diseño, permitiendo no sólo controlar el rango frecuencial de propagación sino hasta cierto punto también sus características eléctricas, es decir la fase de la línea ( $\beta l$ ) y su impedancia característica ( $Z_c$ ).

En el rango de microondas existen básicamente dos formas de obtener estas estructuras. Una consiste en cargar las líneas de transmisión convencionales con elementos reactivos (aproximación

CL). La otra opción es por acople de resonadores a la línea, siendo los resonadores sub-lambda los más utilizados: SRRs o su complementarios CSRRs. En los siguientes subapartados se comentan las dos aproximaciones en mayor detalle, en especial la de tipo resonante, que es la de interés para este trabajo. Ambas aproximaciones se basan en el concepto de líneas de transmisión duales. El nombre de modelo dual obedece a que el circuito equivalente de los elementos que dominan en la zona zurda es el dual del circuito equivalente de una línea de transmisión convencional, ver Fig. 5.

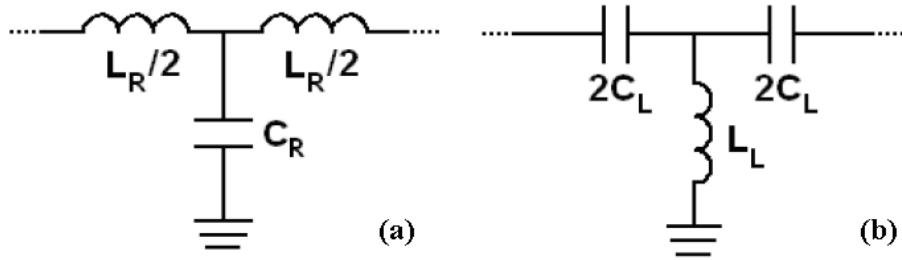


**Fig. 5. (a)** Modelo equivalente para una línea de transmisión convencional (right-handed).  $L_R$  y  $C_R$  son la inductancia serie y capacitancia paralelo del modelo RH TL. **(b)** Modelo equivalente para una línea de transmisión left-handed.  $C_L$  y  $L_L$  son la capacitancia serie e inductancia paralelo del modelo LH TL.

#### I.2.1 LÍNEAS CARGADAS-CL

Un modo de obtener líneas de transmisión metamateriales es cargando una línea de transmisión con una capacitancia serie y una inductancia paralelo, ver Fig. 6. Esta estrategia puede aplicarse a distintos tipos de líneas de transmisión, incluyendo microstrip y guías coplanares.

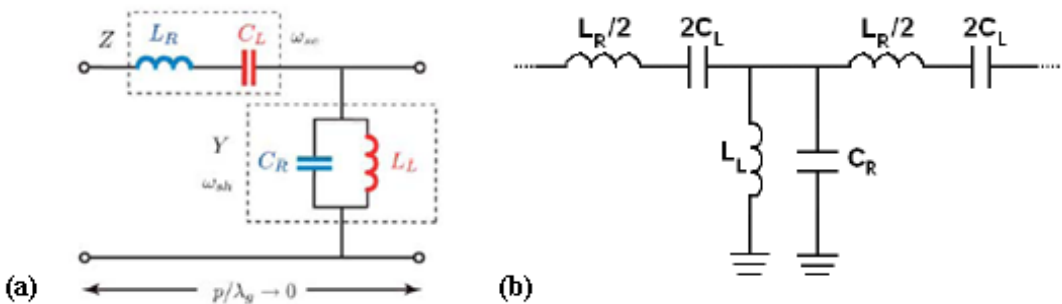


**Fig. 6. (a)** Modelo de un línea de transmisión cargada-CL **(b)** Modelo equivalente al anterior pero en tipo T.

La línea de transmisión obtenida con esta técnica no es puramente dual, dado que el medio introduce elementos parásitos ( $L_R$  y  $C_R$ ). Sin embargo, en cierto rango de frecuencias los elementos de carga ( $L_L$  y  $C_L$ ) son dominantes, dando lugar a un comportamiento zurdo. El comportamiento de este tipo de líneas es múltiple, debido a lo cual se las conoce también en la literatura como líneas de transmisión composite right-left handed (CRLH): a bajas frecuencias left-handed y a altas frecuencias es del tipo right-handed. Estas dos bandas pueden fusionarse en una sola, balanceando para ello la línea de transmisión [4].

Las expresiones de permeabilidad y permitividad efectivas para estas líneas de transmisión son:

$$\mu_{eff} = \frac{L_R}{2l} - \frac{1}{\omega^2 2C_L l} \quad (4)$$

$$\varepsilon_{eff} = \frac{C_R}{2l} - \frac{1}{\omega^2 2L_L l} \quad (5)$$

donde  $l$  representa la longitud de la celda unidad. Para que exista propagación, ambos parámetros han de tener el mismo signo, o de forma equivalente que los signos de las reactancias en serie y paralelo sean opuestos. En la Fig.7, se pueden ver dos tipos de diseños realizados con esta tecnología, que admiten procesos de fabricación planar y son compatibles con circuitos integrados de microondas (MICs).

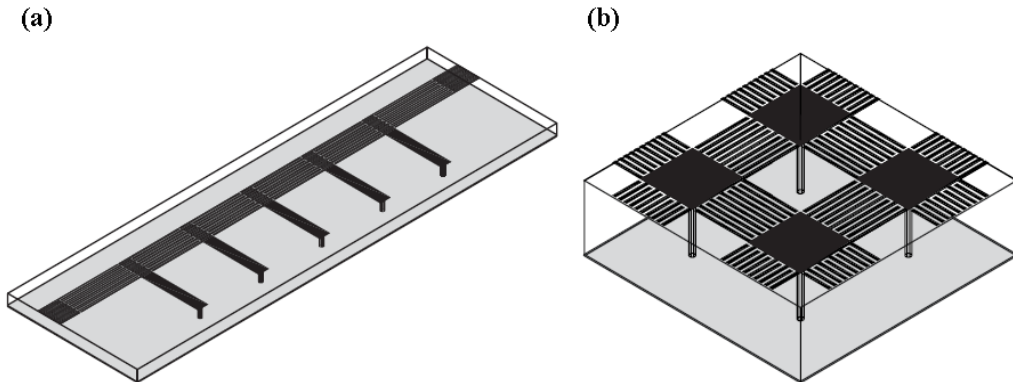


**Fig. 7.** Líneas de transmisión CRLH en tecnología microstrip formada por capacidades interdigitales en serie e inductancias (stub) en paralelo. Las partes de color gris representan el plano de masa y las de color negro metal **(a)** Diseño 1D. **(b)** Estructura tipo seta 2D.

### I.2.2 LÍNEAS DE TIPO RESONANTE

Otro modo de obtener líneas de transmisión metamateriales consiste en combinar alguno de los elementos que forman la línea (capacidad en serie o inductancia en paralelo) con resonadores acoplados a la propia línea de transmisión. Dichos resonadores pueden estar acoplados de distintos modos, dando lugar a diferentes tipos de líneas de transmisión. Como se avanzó con anterioridad, se utilizan principalmente dos tipos de resonadores: metálico (tipo SRR) o su complementario que presenta características duales (tipo CSRR), ver Fig. 8. Al ser las dimensiones de estos resonadores mucho menores que la longitud de onda, permiten la realización de estructuras muy compactas.

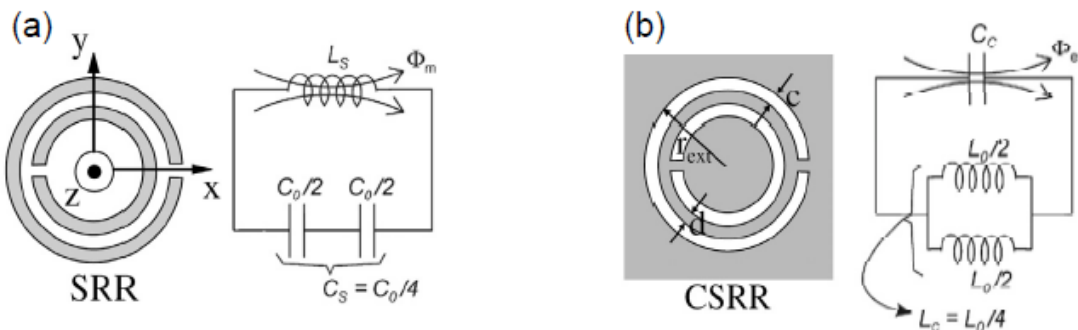


**Fig. 8.** Representación de los tipos principales de resonadores usados, junto al circuito equivalente que modela su comportamiento: **(a)** SRR **(b)** CSRR. Las partes grises indican metalización.

Las propiedades electromagnéticas de estas estructuras resonantes han sido objeto de numerosos estudios [3,5]. La excitación de los resonadores tipo SRR se produce al aplicar un campo magnético axial, mientras que en el tipo CSRR es por campo eléctrico axial.

La primera línea de transmisión de este tipo se implementó en una línea coplanar (CPW) cargada con SRRs y uniones metálicas entre la línea de transmisión y el plano de masa, a modo de inductancias en derivación, ver Fig. 9 [6]. Otra configuración usual con SRRs, consiste en cargar una línea microstrip con capacidades mediante salto (gap) en serie [7].

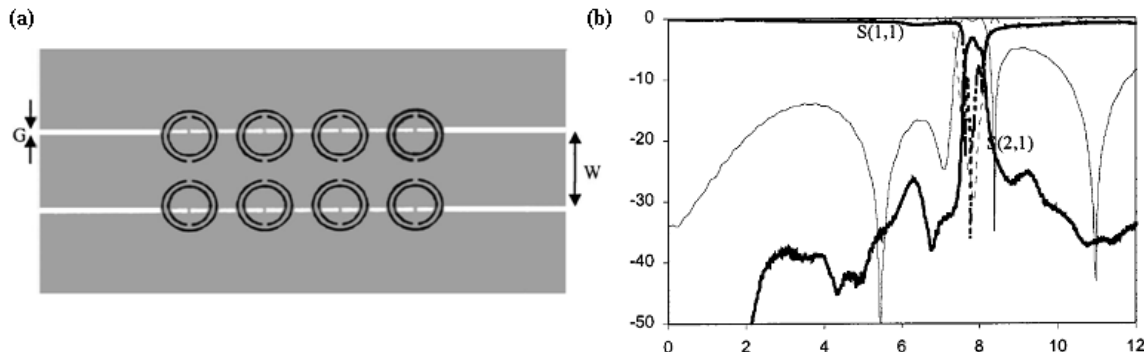


**Fig. 9.** (a) Línea de transmisión de tipo resonante en tecnología coplanar (b) Respuesta en frecuencia.

Los resonadores CSRR presentan ya por si mismos una permitividad negativa, así que pueden ser usados directamente como elementos de carga y rechazan la señal entorno a la frecuencia de resonancia del resonador. En general se suelen grabar en el plano de masa de la línea microstrip, justo por debajo de la tira conductora. Un ejemplo de una implementación real puede verse en la Fig.10, así como los resultados de medir la respuesta de dicho dispositivo [8].

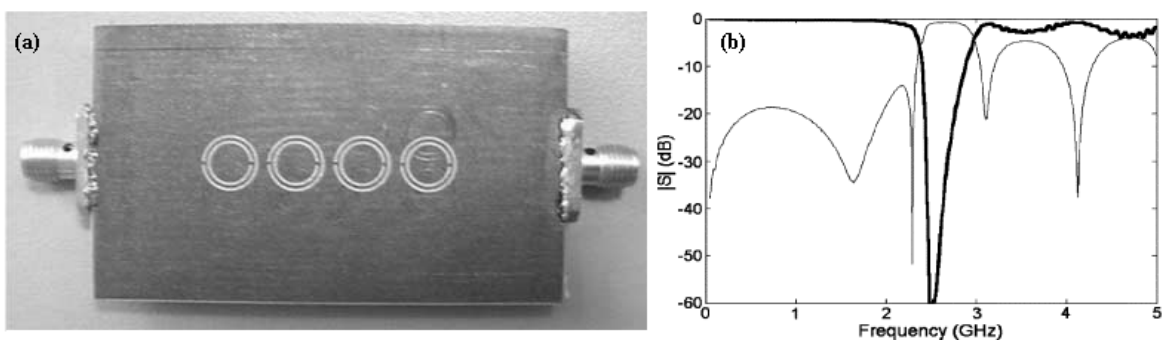


**Fig. 10.** (a) Línea de transmisión de tipo resonante en tecnología microstrip  
(b) Respuesta medida en frecuencia:  $S_{21}$  en línea gruesa,  $S_{11}$  en línea fina.

Las principales aplicaciones de este tipo de líneas son divisores de potencia, filtros paso-banda estrechos o filtros compactos de banda de rechazo. Presentan más flexibilidad de diseño que las líneas de transmisión convencionales para el ajuste de los valores de fase e impedancia característica deseados (en cierto rango frecuencial).

La síntesis no es sencilla, y habitualmente son diseñadores expertos los que la realizan esta tarea con la ayuda de simuladores electromagnéticos de onda completa, combinándolos con métodos de extracción de parámetros circuitales. La optimización directa tiene un gran coste computacional, y

no siempre funciona bien debido al gran número de variables involucradas y a su mutua interdependencia. El Grupo de Aplicaciones de Microondas del iTEAM, en cuyo seno se ha desarrollado este proyecto, había logrado con anterioridad aplicar de forma pionera técnicas basadas en mapeado espacial para el diseño de filtros realizados en tecnología coplanar con SRRs [9], ver Fig.9. Siguiendo esta línea de investigación, se han aplicado técnicas similares para la síntesis de la celda unidad de una línea microstrip cargada con CSRR, ver Fig. 10. En el apartado II se hace un resumen de las técnicas de SM y la versión aplicada en este caso de mapeado espacial agresivo (ASM, del inglés Aggressive Space Mapping) con restricciones. En el apartado IV ya se entra en profundidad en la implementación del algoritmo de diseño automatizado de la celda de estudio descrita en la sección III.

## II. MAPEADO ESPACIAL

Los procedimientos de diseño automatizado (CAD) son prohibitivos en muchos problemas reales, debido a la carga computacional que representan y al uso intensivo que hacen de herramientas de simulación electromagnética (EM). La técnicas de Mapeado Espacial introducidas en 1994 por Bandler et al. [10] supusieron una gran innovación a la hora de elaborar el diseño automatizado de circuitos de microondas, ya que combinan la exactitud de los simuladores EM con la velocidad de los simuladores circuitales, reduciendo de modo considerable el tiempo y la carga computacional.

Tras esa primera versión, numerosas variantes y/o mejoras han ido surgiendo. Una excelente revisión se puede encontrar en [11], aunque desde su publicación ya han aparecido nuevas aproximaciones. El uso de estas técnicas se ha ido consolidando a lo largo de los años, prueba de ello es su aplicación exitosa a distintos tipos de aplicaciones: filtros interdigitales, estructuras de guía de onda 3D, filtros microstrip, componentes RF, diseño de circuitos pasivos en tecnología planar multicapa (LTCC), etc.

Toda estrategia basada en SM asume que la estructura considerada puede simularse usando dos modelos: uno que es complejo y costoso desde el punto de vista computacional aunque preciso llamado modelo fino (fine model), y otro menos exacto pero muy eficiente en términos de CPU llamado modelo grueso (coarse model). La optimización eficiente del modelo fino (simulador EM) se consigue mediante la optimización iterativa del modelo grueso (circuito equivalente).

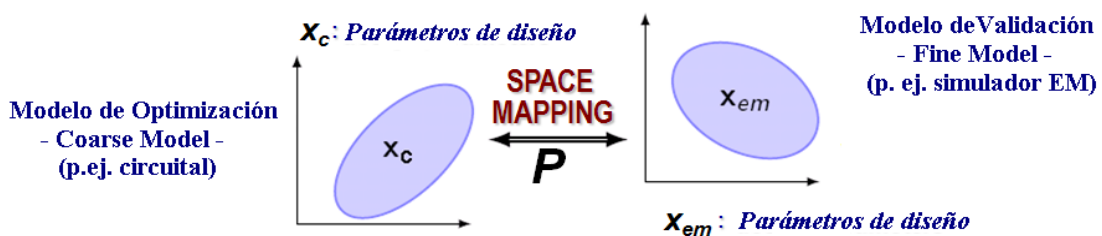


**Fig. 11.-** Esquema del algoritmo SM.

Los algoritmos basados en SM tratan de encontrar la relación de mapeo  $\mathbf{P}$  que relaciona los parámetros que definen al modelo fino o electromagnético, que denotaremos de aquí en adelante por el vector  $\mathbf{x}_{em}$ , con los del modelo grueso o circuital, vector  $\mathbf{x}_c$ , en la región de interés, Fig. 11. Expresado de forma matemática:

$$\mathbf{x}_c = \mathbf{P}(\mathbf{x}_{em}) \quad (6)$$

cumpliéndose en la región de interés:

$$\mathbf{R}_c(\mathbf{P}(\mathbf{x}_{em})) \approx \mathbf{R}_{em}(\mathbf{x}_{em}) \quad (7)$$

donde  $\mathbf{R}_c$  y  $\mathbf{R}_{em}$  son los vectores respuesta correspondientes a los distintos espacios. La solución al problema se obtendrá para la etapa  $j$ -ésima donde:

$$\mathbf{x}_{em}^{(j)} = \mathbf{P}^{-1}(\mathbf{x}_c^*) \quad (8)$$

siendo  $\mathbf{x}_c^*$  el vector grueso que modela la respuesta objetivo a partir de unas especificaciones de diseño dado.

A continuación se enumerarán las distintas etapas que presentan en común toda técnica basada en SM:

- Encontrar un modelo grueso que reproduzca de forma suficientemente fiel la respuesta que presenta la estructura a implementar, proporcionada por el modelo fino.
- Seleccionar la técnica más conveniente al problema a resolver: SM original, ASM, combinación con redes neuronales...
- Obtener las dimensiones que proporcionan la respuesta objetivo con el modelo grueso: vector  $\mathbf{x}_c^*$ .
- Calcular punto inicial en el modelo fino  $\mathbf{x}_{em}^{(0)}$  y simulación del mismo.
- Si la respuesta obtenida cumple las especificaciones de diseño,  $\mathbf{P}(\mathbf{x}_{em}^{(i)}) \approx \mathbf{x}_c^*$ , finalización del algoritmo.
- Extracción de parámetros (PE), obtención de un nuevo punto  $\mathbf{x}_c^{(i)}$ , pesos neuronales...
- Hallar un nuevo punto en el modelo fino  $\mathbf{x}_{em}^{(i)}$  y simulación del mismo, volver al punto 5.

Tras un número determinado de iteraciones se logra la convergencia entre el espacio fino y el grueso. Es conveniente que la respuesta del punto inicial  $\mathbf{x}_{em}^{(0)}$  no se encuentre excesivamente alejado de la solución final, y que el proceso de extracción de parámetros sea lo más eficiente posible.

## II.1. MAPEADO ESPACIAL AGRESIVO

Como se avanzó previamente en el apartado I.2.2, ASM es una evolución de la técnica de mapeado espacial tradicional [12]. Ésta es una estrategia más eficiente, que hace uso de una iteración quasi-Newton junto con la actualización del algoritmo mediante la conocida como fórmula de Broyden. El algoritmo finaliza cuando se encuentra la solución al sistema de ecuaciones no lineales dado por:

$$f(\mathbf{x}_{em}) = \mathbf{P}(\mathbf{x}_{em}) - \mathbf{x}_c^* = 0 \quad (9)$$

Sea  $\mathbf{x}_{em}^{(j)}$  la aproximación j-ésima de la solución a la ecuación dada en (9), el vector  $\mathbf{x}_{em}$  de la siguiente etapa  $\mathbf{x}_{em}^{(j+1)}$ , se calcula como:

$$\mathbf{x}_{em}^{(j+1)} = \mathbf{x}_{em}^{(j)} + \mathbf{h}^{(j)} \quad (10)$$

donde el vector  $\mathbf{h}^{(j)}$  proporciona la longitud de paso en la dirección quasi-Newton y se obtiene resolviendo el sistema lineal:

$$\mathbf{B}^{(j)} \mathbf{h}^{(j)} = -\mathbf{f}(\mathbf{x}_{em}^{(j)}) \quad (11)$$

$\mathbf{B}^{(j)}$  representa la matriz de Broyden para la iteración j-ésima, y se actualiza en cada etapa de acuerdo a la expresión clásica:

$$\mathbf{B}^{(j+1)} = \mathbf{B}^{(j)} + \frac{\mathbf{f}^{(j+1)} \mathbf{h}^{(j)T}}{\mathbf{h}^{(j)T} \mathbf{h}^{(j)}} \quad (12)$$

Para mayor claridad de la evolución del algoritmo, se recoge de forma esquemática la implementación del algoritmo ASM propuesta en [12], ver Fig.12. Este esquema, asume trabajar con el mismo tipo de parámetros en ambos espacios, y por tanto para la inicialización del algoritmo se iguala  $\mathbf{x}_{em}^{(1)}$  a  $\mathbf{x}_c^*$  y la matriz de Broyden inicial a la matriz identidad ( $\mathbf{B}^{(1)}=\mathbf{I}$ ). En caso contrario, habría que estimar a partir de  $\mathbf{x}_c^*$  unas dimensiones de los parámetros que definen a  $\mathbf{x}_{em}^{(1)}$ . A partir de ahí  $\mathbf{x}_{em}$  se actualiza de acuerdo con la ecuación (10) en cada etapa, hasta que se logre convergencia o se alcance el número máximo de iteraciones fijado N.

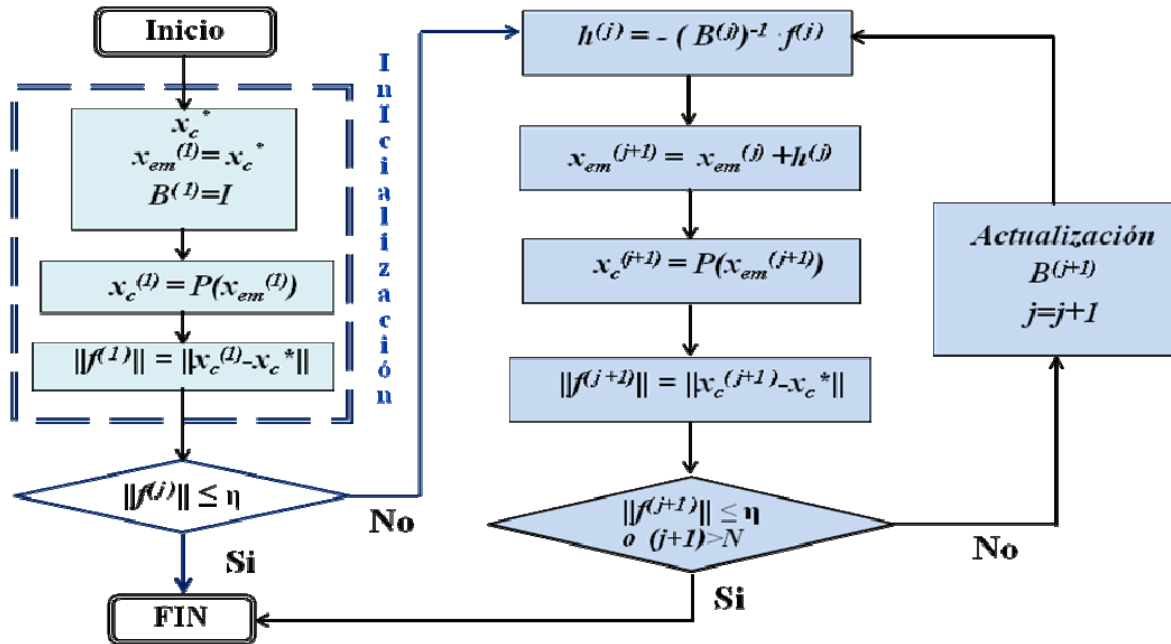


Fig. 12.- Algoritmo de Mapeado Espacial Agresivo.

En nuestro caso, se ha usado una aproximación con restricciones sobre el modelo fino a fin de evitar inestabilidades del algoritmo, y al mismo tiempo reducir el número de simulaciones del modelo fino o electromagnético. Para ello, se definen unos límites para los valores que pueden adoptar los parámetros de  $\mathbf{x}_{em}$ . Si son excedidos, se aplica un decremento en la misma dirección

quasi-newton al paso  $\mathbf{h}^{(i)}$  a usar en (10), hasta que el valor de  $x_{em}$  obtenido esté dentro de la región de confianza. Esta técnica ha sido propuesta con anterioridad en [13].

### III. CELDA DE ESTUDIO

Este trabajo se centra en la síntesis de forma automatizada de líneas microstrip cargadas con CSRR, ver Fig.13. El CSRR considerado es de forma circular, aunque otras topologías como la cuadrada también se hubieran podido elegir. La celda unidad de diseño fue propuesta originariamente por Falcone et al. [8], siendo conocidas tanto su respuesta en frecuencia (filtro de banda de rechazo) como el aspecto del circuito eléctrico equivalente que reproduce su comportamiento en la zona de interés.

Dado que los resonadores CSRR son capaces de inhibir la propagación de una señal dentro de un rango frecuencial, al acoplarlos a la línea de transmisión microstrip sirven para la eliminación de bandas espurias.

#### III.1. TOPOLOGÍA Y MODELO ELÉCTRICO EQUIVALENTE

La celda unidad para el diseño de la estructura, que presenta un valor efectivo de permitividad negativa, se puede observar de forma esquemática en la Fig. 13. En color azul, el resonador CSRR, que está constituido por dos anillos concéntricos abiertos, no metálicos, grabados en el plano de masa de la línea microstrip, justo por debajo de la tira conductora representada en color verde. Los parámetros geométricos que definen la tira metálica superior de la línea microstrip son su anchura  $w$  y su longitud  $l_{strip}$ . Para el caso del CSRR,  $d$  representa la distancia entre los anillos,  $r_{ext}$  el radio externo del CSRR,  $c$  la anchura de las ranuras o slots (se considera la misma en ambos anillos) y  $s_{split}$  el corte realizado a los anillos. El corte aplicado al anillo es aproximadamente un cuadrado de lado  $s_{split}$  de dimensiones similares a la anchura del anillo  $c$ . Con tan sólo cinco parámetros, la topología de la celda queda perfectamente definida

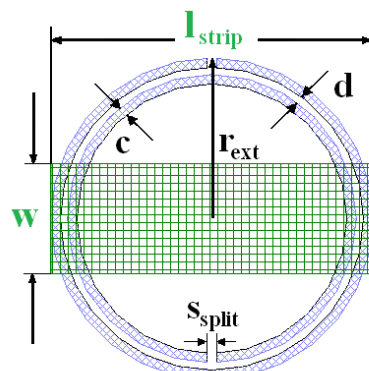


**Fig. 13.-** Celda basada en línea microstrip cargada con CSRR

Dado que el CSRR presenta un tamaño eléctricamente pequeño, es decir el diámetro anillo externo es mucho menor a la longitud de onda  $\lambda$  a la frecuencia de resonancia, puede usarse el modelo de elementos concentrados para simular su comportamiento en la región de interés. El circuito eléctrico equivalente del conjunto, puede observarse en la Fig.14.  $L$  representa la inductancia de la línea microstrip,  $C$  la capacidad de acople entre la línea y el CSRR, y por último el resonador es modelado mediante la combinación de  $L_c$  y  $C_c$  en paralelo. Si se tuvieran en cuenta las pérdidas óhmicas del circuito, habría que añadir una resistencia en paralelo al tanque  $L_c-C_c$  del resonador.

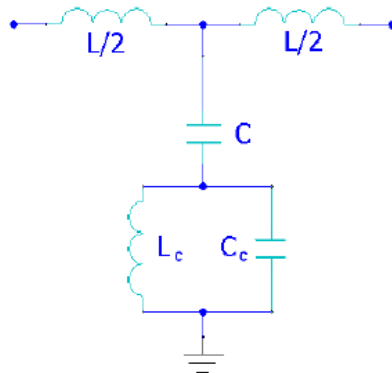


**Fig. 14.**- Circuito eléctrico equivalente de elementos finitos.

El modelo que se acaba de describir, recupera la respuesta obtenida por simulación o medida electromagnética con precisión. Como se avanzó con anterioridad, esta estructura presenta un comportamiento del tipo filtro de banda eliminada o filtro notch. En la Fig. 15, se muestra la respuesta en frecuencia obtenida para un caso particular, de sustrato Rogers RO3010 (con permitividad dieléctrica  $\epsilon_r=10.2$  y espesor  $h=1.27\text{mm}$ ) y con los parámetros geométricos especificados en el pie de figura.

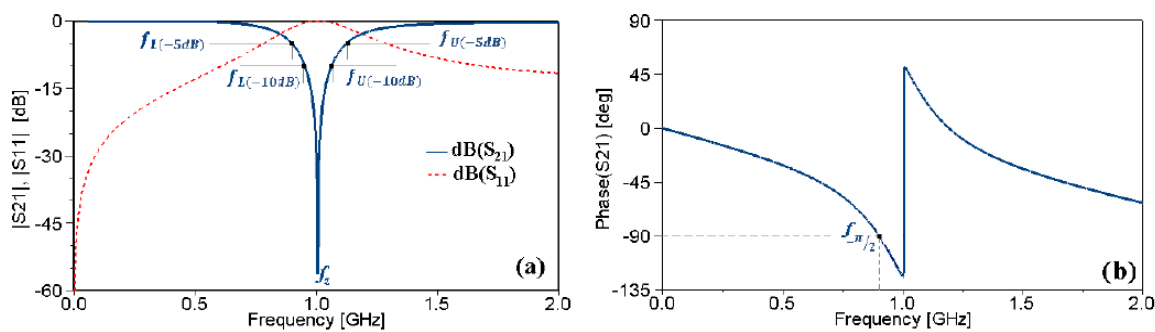


**Fig. 15.-** Respuesta EM de la celda unidad con  $w=3.65$ ,  $l_{\text{strip}}=11.30$ ,  $r_{\text{ext}}=5.65$ ,  $d=0.33$ ,  $c=s_{\text{split}}=0.25$  (Dimensiones en mm): (a) Módulo  $S_{11}$  y  $S_{21}$  (b) Fase  $S_{21}$ .

Existen modelos simples que permiten relacionar los parámetros geométricos del CSRR con sus correspondientes elementos del modelo eléctrico [5]:  $L_c$  y  $C_c$ , ver Fig. 8, o los de la tira microstrip [15]:  $L$  y  $C$ , en Fig. 5. Sin embargo en el modelo completo, Fig.14, al haber acople entre la tira y el CSRR, la aplicación de forma directa de los modelos individuales no permite la obtención correcta

de los parámetros finales. No obstante hay un método que permite su determinación de forma rápida y precisa [14], publicado por Bonache et al. en 2006. En el apartado III.2 se expone este método, ya que ha sido aplicado en la automatización y recoger de forma completa todo el proceso.

El proceso de síntesis es justo el proceso inverso, es decir a partir de la respuesta objetivo, o parámetros circuitales que la modelan, se obtiene la topología física real que presenta aproximadamente esa respuesta electromagnética.

### III.2. EXTRACCIÓN DE PARÁMETROS

Dos frecuencias características son necesarias para la obtención de los parámetros eléctricos, que pueden ser determinadas a través de un simulador electromagnético full-wave o de modo experimental. La primera es la frecuencia que anula la admitancia de la rama en paralelo del circuito eléctrico equivalente, ver Fig.14 y que coincide con la de resonancia del resonador,  $f_0$ :

$$f_0 = \frac{1}{2\pi\sqrt{L_c C_c}} \quad (13)$$

Esta frecuencia puede ser obtenida a través de una representación de la carta de Smith del coeficiente de reflexión  $S_{11}$ , correspondiéndose esta con el punto de intersección de la curva con el círculo unidad. Además al quedar la rama en paralelo en abierto, el valor de la inductancia de la línea se puede calcular a partir del valor imaginario de dicha impedancia, es decir:

$$L = \frac{X_L}{2\pi f_0} \quad (14)$$

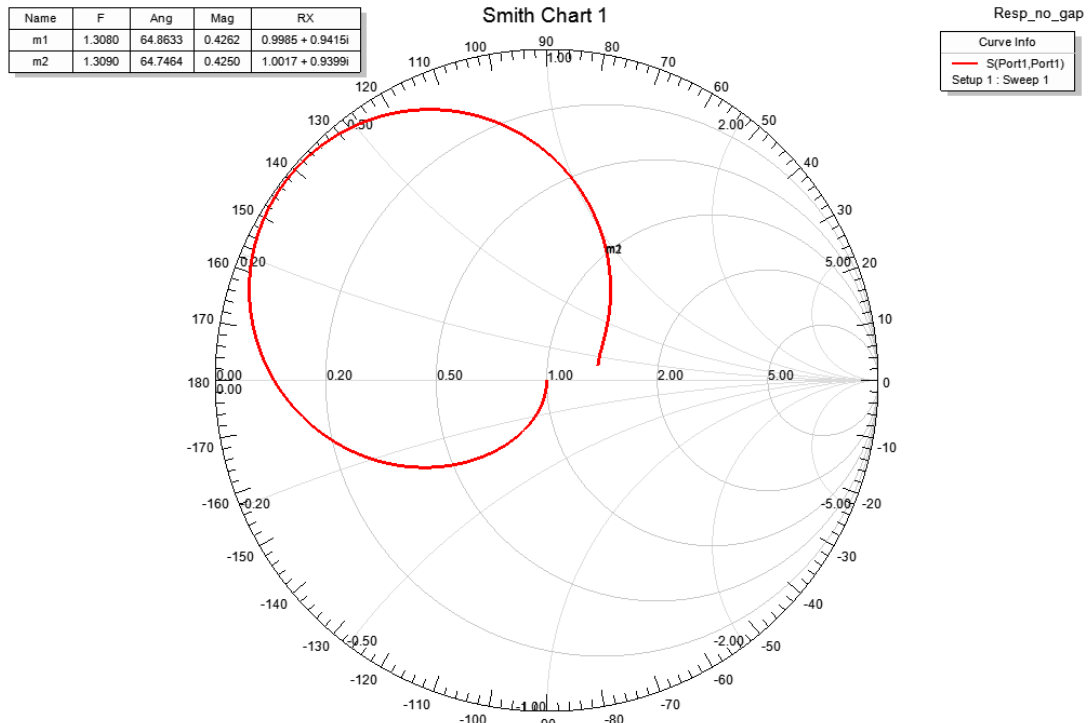


**Fig. 16.-** Representación del coeficiente de reflexión  $S_{11}$  en Carta de Smith. El punto señalado se corresponde a la frecuencia de resonancia del CSRR.

Por otro lado, la frecuencia de cero de transmisión,  $f_z$ , es la que anula la impedancia en derivación y responde a la siguiente expresión:

$$f_z = \frac{1}{2\pi\sqrt{L_c(C + C_c)}} \quad (15)$$

Para determinarla, bastaría la representación del módulo de  $S_{21}$  respecto a la frecuencia, ver Fig. 15.a.

Las expresiones (13) y (15) dependen de tres parámetros. Para determinar únicamente los elementos de la rama en derivación ( $C$ ,  $L_c$  y  $C_c$ ) necesitamos una condición adicional:

$$Z_s(j\omega_{-\pi/2}) = -Z_p(j\omega_{-\pi/2}) \quad (16)$$

donde  $Z_s(j\omega)$  y  $Z_p(j\omega)$  son las impedancias serie y paralelo del circuito en T que modela a la estructura, y  $\omega_{-\pi/2}$  la frecuencia angular donde la fase del coeficiente de transmisión es igual a  $-\pi/2$ , ver Fig. 15.b. Para el presente caso, donde no se consideran pérdidas:

$$Z_p(j\omega) = \frac{1}{j\omega C} + \frac{j\omega L_c}{1 - \omega^2 L_c C_c} \quad (17)$$

$$Z_s(j\omega) = j\omega \frac{L}{2} \quad (18)$$

Resolviendo el sistema de tres ecuaciones y tres incógnitas dado por (13), (15) y (16) se obtienen los parámetros de la rama en paralelo. La aplicación de este método de extracción de parámetros presenta una buena concordancia entre la simulación electromagnética o medida experimental y la del circuito eléctrico equivalente [14].

#### IV. AUTOMATIZACIÓN

El propósito de este trabajo es encontrar una metodología basada en ASM para la generación de forma automática de la geometría de la celda bajo estudio, y que sirva de base para afrontar futuros trabajos de diseños con líneas de transmisión artificiales más complejas.

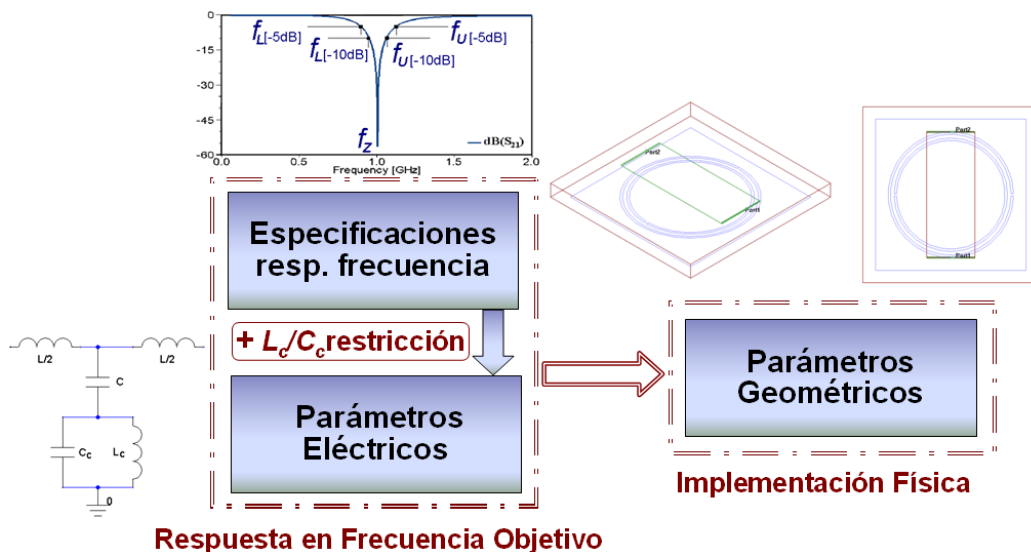


**Fig. 17.-** Diagrama esquemático del problema a resolver.

Para resolver este problema, bien se parte de unas especificaciones de la respuesta objetivo en frecuencia o de un conjunto de parámetros circuitales que modelen esa respuesta. En el caso de tener que calcular los elementos del circuito equivalente, es necesario tener en cuenta que la solución sea implementable físicamente. Para ello se ha de establecer un rango de validez del cociente ( $L_c/C_c$ ) a la hora del cálculo de los parámetros circuitales, similar al deducido en el artículo de J. Bonache et al. [15], para garantizar que el CSRR sea realizable.

#### IV.1. PLANTEAMIENTO

En los apartados anteriores se ha visto con detalle tanto la celda de diseño, como las técnicas de ASM para automatizar su síntesis. Habría distintas formas de aplicación de dichas técnicas, en función de si se trabaja con:

- Los mismos parámetros en ambos espacios (dimensiones físicas). En ese caso el valor inicial de la matriz de Broyden se toma igual a la identidad.
- Parámetros distintos en cada espacio (circuitales para el modelo grueso y físicas en el modelo fino). La aproximación inicial de la matriz de Broyden como matriz identidad no parece la más adecuada y para acelerar la convergencia a su valor final se ha propuesto una inicialización distinta basada en un esquema de diferencias finitas.

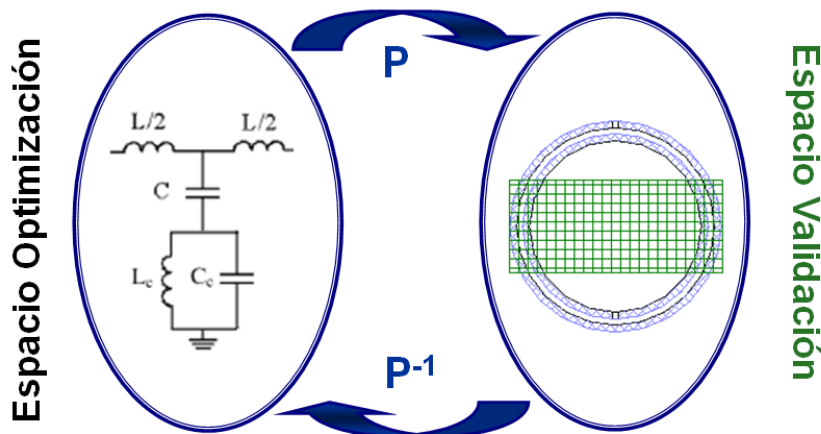


**Fig. 18.-** Espacios diferenciados para la aplicación de ASM.

La opción que se logró implementar con éxito fue la segunda, con parámetros distintos en ambos espacios. El vector  $x_c$  que caracteriza al modelo circuital o grueso, es un vector de cuatro componentes:  $L$ ,  $C$ ,  $L_c$  y  $C_c$ . Con el fin de que la resolución del problema se simplifique al máximo, parece que lo más adecuado sería tener el mismo número de parámetros en el modelo fino para que la matriz de Broyden sea cuadrada (y por tanto fácilmente invertible). Se realizan entonces las siguientes asunciones:

- El corte de los anillos  $s_{split}$  se fija al grosor del slot que forman los anillos, pues en el estudio paramétrico se observa que no tiene gran influencia en la respuesta y los modelos teóricos como el de Marqués [5] no lo tienen en cuenta.

- La longitud de la tira conductora de la línea microstrip se toma dos veces el radio externo  $r_{ext}$ . Longitudes menores harían que el circuito equivalente dejara de ser válido pues habría distinto acople, y se debería tener en cuenta líneas de acceso para la medida y su transición, dejando también de ser válido el PE propuesto. Longitudes mayores no tienen influencia significativa en la respuesta final, pues el acople entre la línea y el CSRR es el mismo y además presenta mayor interés un diseño que sea lo más compacto posible.

De este modo se consigue reducir el número de parámetros efectivos que caracterizan a  $x_{em}$  a cuatro:  $w_{strip}$ ,  $r_{ext}$ ,  $c$  y  $d$ .

#### IV.2. IMPLEMENTACIÓN DEL MÉTODO

El método para la obtención de la síntesis automatizada ha sido implementado en Matlab. Las simulaciones del modelo circuital y electromagnético precisan de herramientas software adicionales específicas, que serán controladas desde Matlab por medio de scripts. En nuestro caso, la simulación del modelo fino se ha hecho con Ansoft Designer, pero otros simuladores EM como Agilent Momentum (empleado por otros grupos de investigación) también servirían igualmente. Se precisa además emplear un modelo circuital. Ansoft Designer tiene integrado un módulo (Nexxim) que permite realizar esta simulación de manera casi instantánea. La llamada a Designer se realiza mediante scripts desde Matlab.

##### IV.2.1 INICIALIZACIÓN

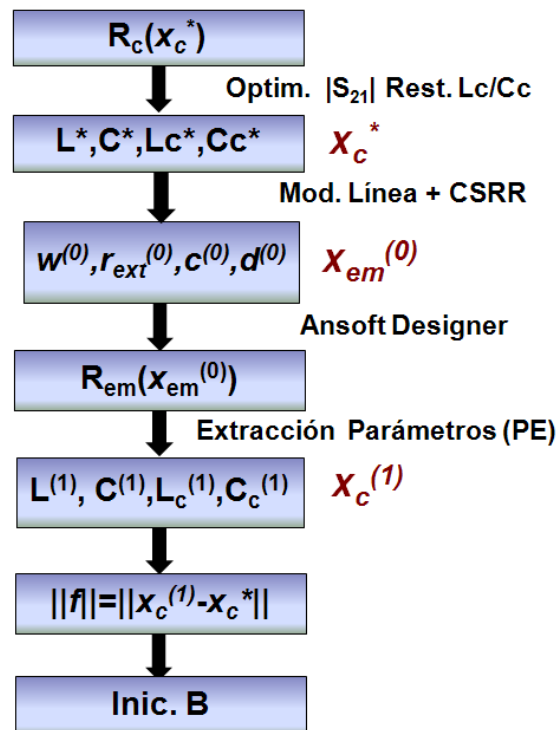


**Fig. 19.-** Esquema de inicialización del algoritmo.

El punto de partida es la respuesta objetivo  $R_c(\mathbf{x}_c^*)$ . Esta puede venir dada directamente por los valores del circuito equivalente si son conocidos a priori, es decir el vector  $\mathbf{x}_c^* = [L^*, C^*, L_c^*, C_c^*]$ . De lo contrario,  $\mathbf{x}_c^*$  se determinará resolviendo un sistema de ecuaciones no lineales a partir de unas especificaciones en frecuencia de la respuesta objetivo: la frecuencia cero de transmisión  $f_z$ , y las frecuencias que definen el ancho de banda a -10 dB ( $f_{L(-10dB)}$ ,  $f_{U(-10dB)}$ ) y a -5 dB ( $f_{L(-5dB)}$ ,  $f_{U(-5dB)}$ ) del parámetro  $S_{21}$ . A este sistema hay que imponerle varias restricciones para que tenga solución realizable, y que se obtendrá usando la herramienta de optimización de Matlab: Optimtool. Todas las componentes de  $\mathbf{x}_c^*$  han de ser positivas y además no cualquier cociente  $L_c^*/C_c^*$  es válido. En el artículo de referencia [16], se ha determinado el rango  $900 \leq (L_c/C_c)[\text{H/F}] \leq 1600$  como válido. Este es el límite establecido para CSRRs cuando la anchura de los slots es igual a la distancia entre los anillos del CSRR ( $c=d$ ). Para nuestro caso, la solución encontrada puede superar esos márgenes, aunque ha de estar en ese orden de valores.

El siguiente paso, ver Fig. 19, consiste en encontrar una geometría inicial para la celda unidad, es decir  $\mathbf{x}_{em}^{(0)}$ . Para la determinación de las dimensiones del CSRR, se hace uso del programa CSRR.exe que calcula la frecuencia de resonancia y parámetros eléctricos del resonador siguiendo las expresiones recogidas en el artículo de Baena et al. [5], para unas dimensiones físicas y del sustrato determinadas. La capacidad del resonador CSRR,  $C_c$ , es aproximadamente igual a la de un disco metálico de radio  $a = r_0 - c/2$  rodeado por un plano de masa da una distancia  $b-a = c$ , siendo  $r_0$  el radio medio del CSRR, ver Fig.20. Por otro lado, la inductancia  $L_0$ , Fig. 8, es la de una guía coplanar circular de longitud  $2\pi r_0$ , con anchura de la tira  $d$  y del slot  $c$ , siendo la inductancia del resonador  $L_c = 4L_0$  [17].

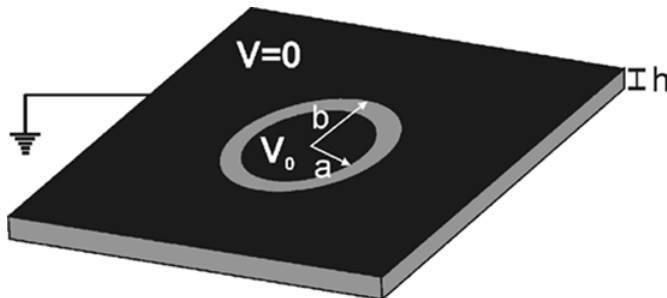


**Fig. 20.-** Modelo para calcular la capacidad del CSRR. El sustrato está caracterizado por una permitividad  $\epsilon$  y por un espesor  $h$

Con la función de Matlab “fminsearch” se calculan esos valores geométricos que presentan una  $L_c$  y  $C_c$  que minimizan la siguiente función de error

$$f_{error} = \frac{\sqrt{(L_c - L_c^*)^2 + (C_c - C_c^*)^2}}{\sqrt{(L_c^*)^2 + (C_c^*)^2}} \quad (19)$$

Si no se fija ninguna de las dimensiones que caracterizan al resonador ( $c, d, r_{ext}$ ), habrá múltiples soluciones. En nuestro caso se ha optado por fijar  $c = 0.25\text{mm}$ , y calcular  $d$  y  $r_{ext}$ , obteniéndose así una solución determinista. Este valor es razonable, ya que si  $c$  fuese menor de  $0.15\text{mm}$  el CSRR no

podría fabricarse fácilmente, y un valor de  $c$  muy grande supondría unas dimensiones del CSRR demasiado grandes para considerarlo eléctricamente pequeño. El punto inicial va a condicionar la evolución: el número de iteraciones del algoritmo variará, e incluso no tiene porque alcanzarse el mismo punto de convergencia. Además si la respuesta obtenida al simular el punto inicial está muy alejada de la objetivo, puede llevar incluso a la no convergencia del método.

Queda por determinar la anchura de la tira microstrip, ya que el valor de longitud se aproxima directamente a  $2r_{ext}$ , como se argumentó en la sección IV.1. El valor de  $w$  se calcula a partir de las expresiones de una línea microstrip de impedancia característica  $Z_c$  conocida [15], inferida a partir de los valores de  $L^*$  y  $C^*$ :

$$Z_c = \sqrt{\frac{L_{pul}}{C_{pul}}} = \sqrt{\frac{L^*}{C^*}} \quad (20)$$

donde  $L_{pul}$  y  $C_{pul}$  son la inductancia y capacitancia por unidad de longitud.

$$Z_c = \begin{cases} \frac{60\pi}{\sqrt{\epsilon_{eff}}} \ln\left(\frac{8h}{w} + \frac{w}{4d}\right) & \text{Si } \left(\frac{w}{h}\right) \leq 1 \\ \frac{120\pi}{\sqrt{\epsilon_{eff}} \cdot \left[w/h + 1.393 + 0.667 \cdot \ln\left(w/h + 1.444\right)\right]} & \text{Si } \left(\frac{w}{h}\right) \geq 1 \end{cases} \quad (21)$$

$$\epsilon_{eff} = \frac{\epsilon_r + 1}{2} + \frac{\epsilon_r - 1}{2} \frac{1}{\sqrt{1 + 12 \frac{h}{w}}} \quad (22)$$

siendo  $\epsilon_r$  y  $h$  la permitividad dieléctrica y el espesor del sustrato respectivamente. Ya tendríamos entonces calculado  $\mathbf{x}_{em}^{(0)} = [w, r_{ext}, 0.25, d]$  y se llamaría a Designer para obtener su respuesta en frecuencia  $R(\mathbf{x}_{em}^{(0)})$ . Aplicando directamente la técnica de extracción de parámetros detallada en III.2 se obtendría  $\mathbf{x}_c^{(1)}$  y se podría calcular la función error, del siguiente modo:

$$\|f^{(i)}\| = \|\mathbf{x}_c^{(i)} - \mathbf{x}_c^*\| = \sqrt{(L^{(i)} - L^*)^2 + (C^{(i)} - C^*)^2 + (L_c^{(i)} - L_c^*)^2 + (C_c^{(i)} - C_c^*)^2} \quad (23)$$

La inicialización clásica de la matriz de Broyden  $B$  sería con la matriz identidad, pero dado que estamos usando distinta clase de variables en cada espacio, y con objeto de acelerar la convergencia del algoritmo, se propone una inicialización diferente.

$$B^{(1)} = \begin{pmatrix} \frac{\partial L}{\partial w} & \frac{\partial L}{\partial r_{ext}} & \frac{\partial L}{\partial c} & \frac{\partial L}{\partial d} \\ \frac{\partial C}{\partial w} & \frac{\partial C}{\partial r_{ext}} & \frac{\partial C}{\partial c} & \frac{\partial C}{\partial d} \\ \frac{\partial L_c}{\partial w} & \frac{\partial L_c}{\partial r_{ext}} & \frac{\partial L_c}{\partial c} & \frac{\partial L_c}{\partial d} \\ \frac{\partial C_c}{\partial w} & \frac{\partial C_c}{\partial r_{ext}} & \frac{\partial C_c}{\partial c} & \frac{\partial C_c}{\partial d} \end{pmatrix} \quad (24)$$

Para calcular la primera columna de  $B$ , o variación de  $\mathbf{x}_c$  con la anchura de la tira microstrip  $w$ , se perturba ligeramente  $w$ , es decir  $\mathbf{x}_{em}^{(p)} = [w + \Delta w, r_{ext}, c, d]$ . Esa nueva configuración se simula con Ansoft Designer y se deduce un nuevo conjunto de valores de los parámetros circuitales:  $L^{(p)}, C^{(p)}$ ,

$L_c^{(p)}$  y  $C_c^{(p)}$  haciendo uso del citado método de extracción de parámetros. A continuación se aplica el siguiente esquema de diferencias finitas:

$$\begin{aligned}\frac{\partial L}{\partial w} &\approx \frac{L^{(p)} - L^*}{(w^* + \Delta w) - w^*} \approx \frac{L^{(p)} - L^*}{w^{per} - w^*} \\ \frac{\partial C}{\partial w} &\approx \frac{C^{(p)} - C^*}{(w^* + \Delta w) - w^*} \approx \frac{C^{(p)} - C^*}{w^{per} - w^*} \\ \frac{\partial L_c}{\partial w} &\approx \frac{L_c^{(p)} - L_c^*}{(w^* + \Delta w) - w^*} \approx \frac{L_c^{(p)} - L_c^*}{w^{per} - w^*} \\ \frac{\partial C_c}{\partial w} &\approx \frac{C_c^{(p)} - C_c^*}{(w^* + \Delta w) - w^*} \approx \frac{C_c^{(p)} - C_c^*}{w^{per} - w^*}\end{aligned}\quad (25)$$

Se procedería de igual modo para el resto de componentes de  $\mathbf{x}_c$ . Por tanto, se necesitan cuatro simulaciones electromagnéticas para la inicialización de la matriz  $B$ . Comentar también que no se perturban todas las componentes por igual, pues todas las dimensiones geométricas no son del mismo orden. Por ejemplo la perturbación del slot que conforma el anillo de valor  $c$ , lógicamente va a ser mucho menor que la del radio externo del resonador  $r_{ext}$ . Se aplica un incremento porcentual distinto en función de la dimensión considerada.

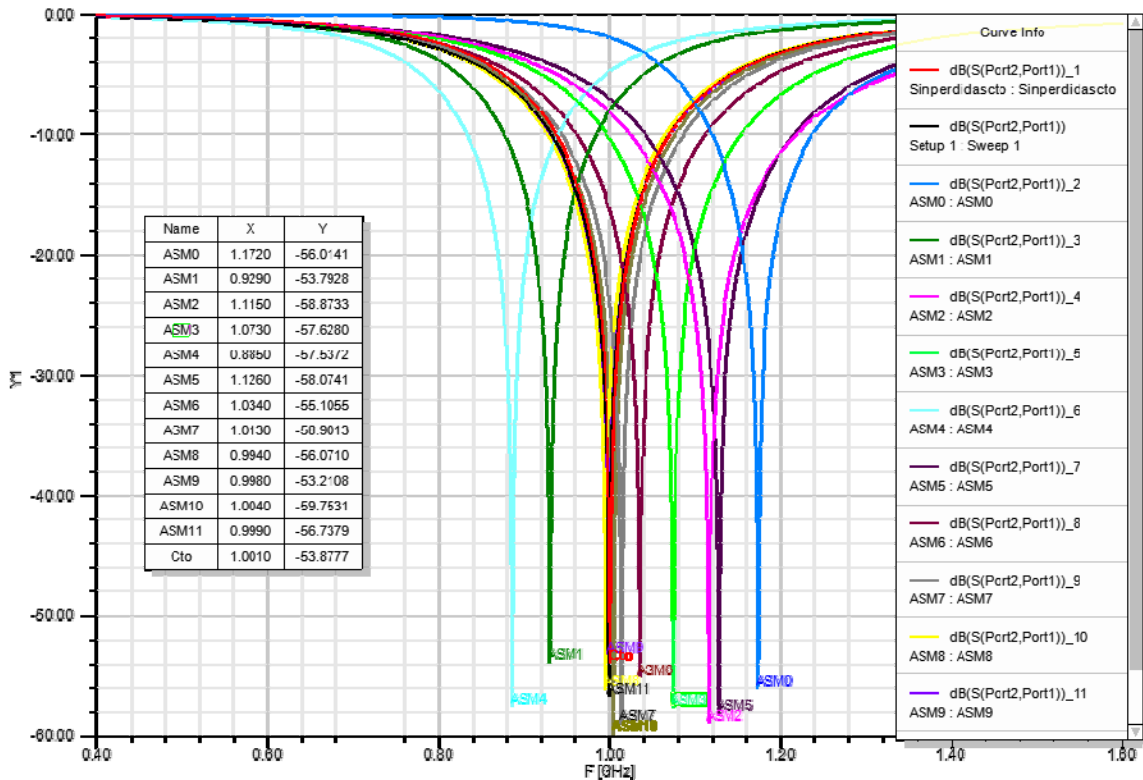


**Fig. 21.-** Evolución del algoritmo para un caso práctico de la celda de estudio.

A matrices iniciales distintas, el desarrollo del algoritmo variará, bien sea por alcanzar distintos valores de convergencia (aunque en general similares) o bien en el número de iteraciones necesarios para alcanzar convergencia. Esto se debe a que la evolución del algoritmo no tiene

porque ser siempre linealmente descendente con respecto al error, si bien es verdad que conforme avanza el algoritmo la respuesta del modelo fino se va alineando con la del objetivo, como se puede apreciar en la Fig. 21.

La matriz  $B$  en posteriores iteraciones se actualiza con la fórmula clásica de Broyden (12), el proceso de diferencias finitas sólo es para la etapa de inicialización.

#### IV.2.2 DIAGRAMA DE FLUJO

Las técnicas de ASM fueron introducidas con anterioridad en el apartado II.1, que son las que se han aplicado, aunque en este caso una versión con restricciones [13] para evitar inestabilidades del algoritmo, ver zona resaltada en rojo del esquema global del método Fig. 22. Se definen entonces unos límites a los parámetros geométricos de la celda  $[x_{em\_min}, x_{em\_max}]$ . Dimensiones muy pequeñas o negativas son de difícil fabricación o carecen de sentido físico, y si son excesivamente grandes el modelo eléctrico equivalente considerado, ver Fig. 14, deja de ser válido, con lo que la extracción de parámetros es ineficiente y la convergencia de ASM se ve comprometida. Antes de proceder a simular el nuevo modelo electromagnético obtenido tras la actualización de la matriz de Broyden, se ha de comprobar que este pertenezca a la región de confianza, es decir  $x_{em\_min} \leq x_{em\_test} \leq x_{em\_max}$ . Si no es así, hay que aplicar un decremento  $\delta$  en la dirección quasi-newton al paso  $h^{(j)}$ , de forma iterativa hasta que el valor de  $x_{em\_test}$  obtenido se encuentre dentro de los límites. Ese factor  $\delta$ , obviamente entre cero y uno, es fijo durante la ejecución y se adopta típicamente el valor entre 0.3 y 0.4. Una vez obtenido un  $x_{em\_test}$  válido, se actualiza  $x_{em}^{(j+1)} = x_{em\_test}$  y se sigue con la evolución normal del algoritmo.

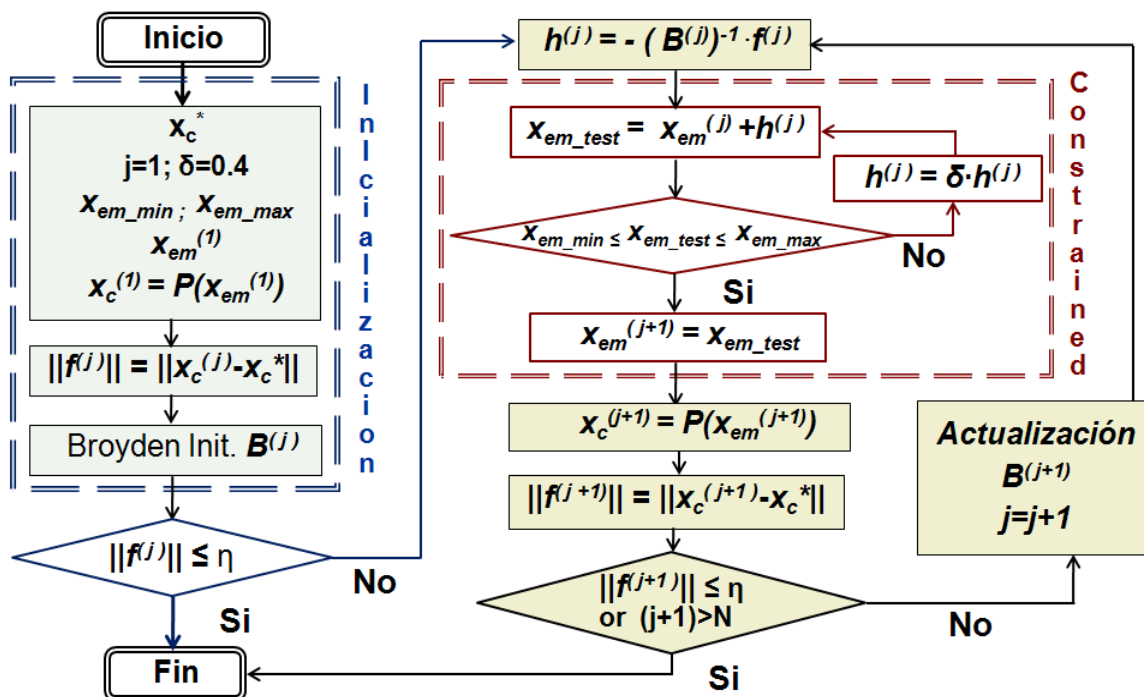


Fig. 22.- Diagrama completo para la obtención de la síntesis de la estructura.

La condición de salida es que el número de iteraciones alcanzado sea mayor que  $N$  o que se alcance convergencia, es decir que la norma de la función de error (23) sea menor que un determinado  $\eta << 1$ .

#### IV.2.3 ESTRUCTURA DEL CÓDIGO

Se comenta brevemente como está organizado el código fuente, de cara a facilitar su consulta o modificación posterior. El programa principal se llama: *ASM\_2E\_PEBCNwrdl.m*. Las principales funciones a las que llama son

- **function escribir\_datos\_entrada(L,C,L<sub>c</sub>,C<sub>c</sub>,h,eps\_r)**: Genera un fichero (Entrada.txt), donde se introducen datos a utilizar otras funciones, para estimar parámetros físicos. Valores circuitales modelan respuesta objetivo  $L^*$ ,  $C^*$ ,  $L_{c}^*$ ,  $C_{c}^*$  y características del sustrato a realizar implementación física:  $\epsilon$ ,  $h_{dielectrico}$ .
- **function x = Calcula\_wrd**: Estimación del punto inicial para el modelo fino, es decir las dimensiones físicas del anillo ( $r_{ext}, d$ ),  $c = 0.25\text{mm}$  y la tira ( $w$ ; pues  $l_{strip}$  se estima como  $2r_{ext}$ ). Hace uso de:
  - **function y = LCopt\_rd(dat)**: Se usa para calcular a partir de  $L_c$ ,  $C_c$  las dimensiones del resonador con ayuda del programa CSRR.exe.
  - **function y = calc\_wstrip(w)**: Estima a partir de  $L$ ,  $C$  la dimensión de la anchura de la tira microstrip  $w$  aplicando fórmulas del Pozar [15].
  - **function EM\_Designer\_2E\_PEBCN(x)**: Evaluación de  $x_{em}$  Esta función genera el script necesario para hacer una llamada a Designer desde Matlab y obtener la respuesta EM en frecuencia de **Celda\_singap.adsn**. Ficheros de datos exportados para posterior procesado en Matlab: Smith.csv, ModuloS21.csv y FaseS21.csv.
- **function [L,C,L<sub>c</sub>,C<sub>c</sub>]=Procesa\_mod**: Extracción de parámetros según [14]. Las funciones siguientes se llaman durante su ejecución:
  - **function [L,f<sub>0</sub>]=lee\_Smith(ruta)**: Calcula parámetro  $L$  del circuito eléctrico equivalente, a partir de procesado archivo Smith.csv (representación de la carta de Smith del coeficiente de reflexión  $S_{11}$ ) con **lectura\_archivo\_S11.m**.
  - **function S21= lee\_archivo(ruta)**: Función para poder operar en Matlab con modulo y fase de  $S_{21}$ , simulados en Ansoft Designer y exportados en ModuloS21.csv y FaseS21.csv
  - **function y = escribir\_datos(f<sub>0</sub>,f<sub>z</sub>,f<sub>m90</sub>,L)**: Genera fichero *Dat\_param.txt* con los datos a usar luego por **f\_extract** para cálculo de  $C$ ,  $L_c$ ,  $C_c$ .
  - **function y = f\_extract(x)**: Definición del sistema de ecuaciones para la extracción parámetros circuitales a resolver con función de Matlab **fsolve**.

## V. RESULTADOS

Los ejemplos que se muestran a continuación se han publicado en el artículo presentado recientemente en el International Microwave Symposium 2010, a fin de ilustrar las capacidades del método implementado para la obtención automatizada de la síntesis de la celda de interés. El sustrato utilizado es el comercial Rogers RO3010 de permitividad dieléctrica  $\epsilon_r=10.2$  y de espesor  $h=1.27\text{mm}$ , para todos los casos. Comentar además que el número máximo de iteraciones que se toma es  $N=50$  y que la dimensión más pequeña aceptada como válida para los parámetros físicos es de 0.15 mm (por requisitos de fabricación) y el radio externo del resonador CSRR nunca superior a 8mm.

Los ejemplos realizados han sido ejecutados en un ordenador estándar de 3GB de RAM y un procesador a 2.86GHz. El tiempo de ejecución de una simulación EM es de aproximadamente 90 segundos y el de la síntesis completa alrededor de 25-30 minutos de media. Si no se contara con una técnica de extracción de parámetros directa, la síntesis automatizada se vería ralentizada notablemente y se pasaría de un tiempo de computación de minutos a múltiples horas.

### V.1. EJEMPLO DE VALIDACIÓN

Para el primer ejemplo, se parte de la repuesta óptima circuital proporcionada en [14] y así poder validar al mismo tiempo la técnica utilizada.

	$L[\text{nH}]$	$C[\text{pF}]$	$L_c[\text{nH}]$	$C_c[\text{pF}]$
$x_c^*$	5.08	4.43	2.98	4.06
$x_c^{(22)}$	5.08	4.43	2.98	4.05

**Tabla 1.-** Valor de  $x_c^*$  y  $x_c^{(22)} \approx P(x_{em}^{(22)}) = P(x_{em}^*)$ .

La estimación inicial de las dimensiones de la celda,  $x_{em}^{(1)}$ , hacen que la respuesta se vaya a frecuencias más altas que la respuesta objetivo determinada a partir de  $x_c^*$ . El cero de transmisión pasa de estar a 1GHz a 1.176GHz, ver Fig. 23. Sin embargo, tras veintidós iteraciones se logra alinear ambas respuesta con un ajuste casi perfecto.

	$r_{ext}[\text{mm}]$	$c[\text{mm}]$	$d[\text{mm}]$	$w[\text{mm}]$	$l_{strip}[\text{mm}]$
$x_{em}^{(1)}$	6.39	0.25	0.95	2.43	12.78
$x_{em}^* = x_{em}^{(22)}$	5.68	0.36	0.33	4.97	11.36

**Tabla 2.-** Valores de las dimensiones de la celda: estimación inicial  $x_{em}^{(1)}$  y final, tras aplicar ASM  $x_{em}^*$ .

Puede observarse en la Tabla 1, que al hacer la extracción de parámetros de la solución final, los valores calculados coinciden prácticamente con los mismos que modelan la respuesta objetivo de partida. El valor de la norma error  $\eta$  es de tan sólo 0.015 (23) para esa etapa, aunque ya se logran valores pequeños a partir de la iteración número diez, si bien se ha dejado evolucionar al algoritmo hasta conseguir el valor de error mínimo.

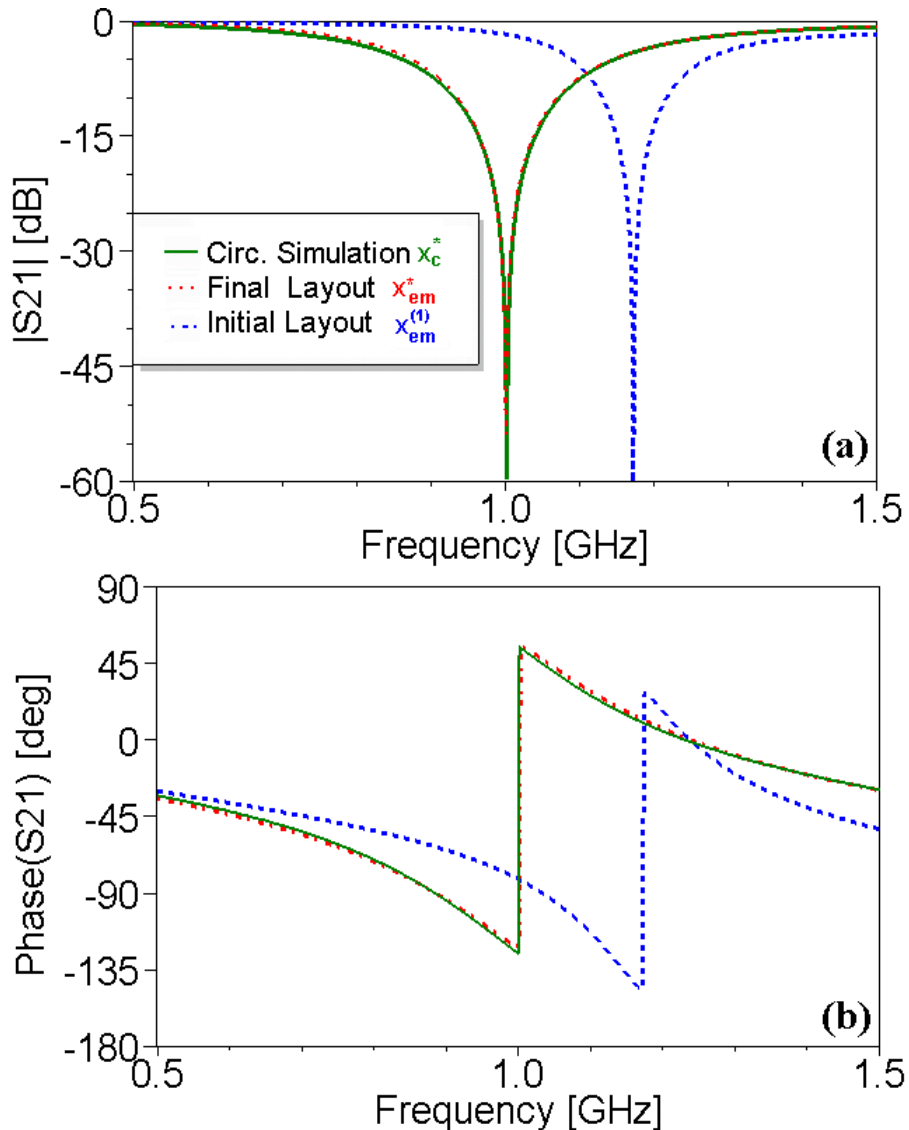


**Fig. 23.-** Módulo (a) y fase (b) del coeficiente de transmisión  $S_{21}$  para la celda de estudio. Representada en verde, la traza correspondiente a la respuesta objetivo  $x_c^*$ ; en azul y trazo discontinuo la solución inicial  $x_{em}^{(1)}$  y punteada en rojo la solución final  $x_{em}^*$ .

Los valores de geometría finales  $x_{em}^*$  son muy parecidos a los publicados en el artículo [14], aunque no iguales. La solución no es única, pues se ha comprobado con otros grupos con los que se colabora en la resolución de este problema que técnicas similares pero distintas herramientas software se llega también a otras posibles soluciones implementables.

#### V.1. EJEMPLO DE APLICACIÓN

En este segundo ejemplo, la respuesta objetivo presenta el cero de transmisión  $f_z$  a una frecuencia más alta, concretamente a 1.6 GHz, y se obtiene un diseño final mucho más compacto, ver resultados en Tabla 2. La solución final se alcanza tras 16 iteraciones, siendo el ajuste entre respuesta objetivo y solución final también bueno, como se observa en la Fig. 24, aunque algo peor que en el caso anterior.

	$L[\text{nH}]$	$C[\text{pF}]$	$L_c[\text{nH}]$	$C_c[\text{pF}]$
$x_c^*$	4.86	1.88	2.18	2.89
$x_c^{(16)}$	4.87	1.89	2.15	2.91

Tabla 3.- Valor de  $x_c^*$  y  $x_c^{(16)} \approx P(x_{em}^{(16)}) = P(x_{em}^*)$ .

	$r_{ext}[\text{mm}]$	$c[\text{mm}]$	$d[\text{mm}]$	$w[\text{mm}]$	$l_{strip}[\text{mm}]$
$x_{em}^{(1)}$	4.83	0.25	0.93	1.16	9.66
$x_{em}^* = x_{em}^{(16)}$	4.01	0.43	0.15	1.94	8.02

Tabla 4.- Valores de las dimensiones de la celda: estimación inicial  $x_{em}^{(1)}$  y final, tras aplicar ASM  $x_{em}^*$ .

En la Fig. 25 se ha representado la evolución del error con las iteraciones del algoritmo, constatándose como se ha señalado anteriormente no tiene que bajar linealmente el error. Si se realiza la ejecución con  $\delta=0.3$  en lugar del usado para este caso  $\delta=0.4$ , se obtienen dimensiones similares pero con un error ligeramente superior.

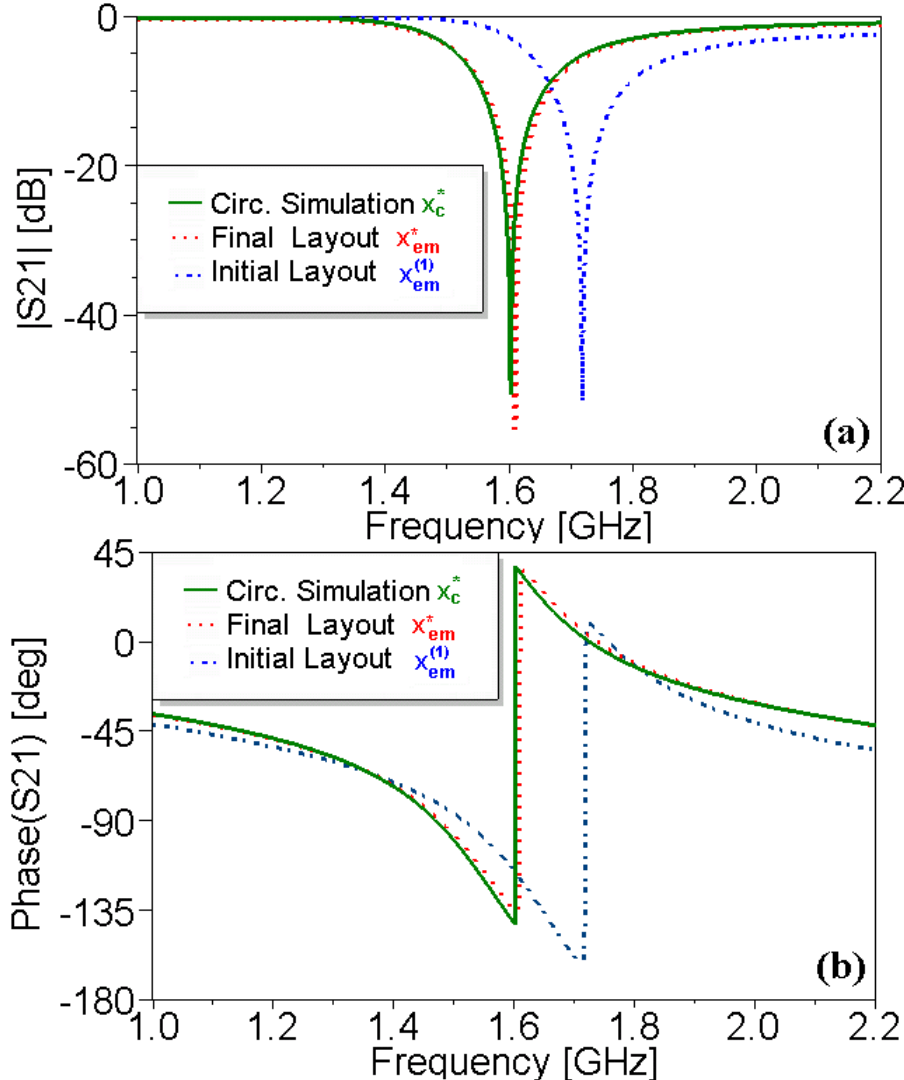
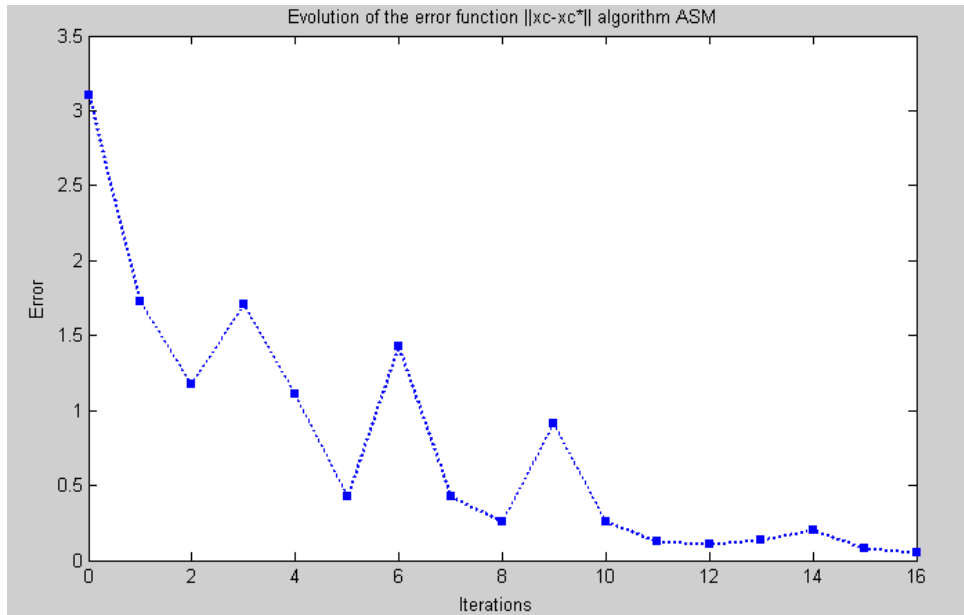


Fig. 24.- Módulo (a) y fase (b) del coeficiente de transmisión  $S_{21}$  para la celda de estudio. Representada en verde, la traza correspondiente a la respuesta objetivo  $x_c^*$ ; en azul y trazo discontinuo la solución inicial  $x_{em}^{(1)}$  y punteada en rojo la solución final  $x_{em}^*$ .



**Fig. 25.-** Evolución del error con las etapas.

## VI. CONCLUSIONES

Se ha demostrado que las técnicas son útiles para la generación automática de la celda unidad de una línea microstrip cargada con CSRR. Dado un conjunto de especificaciones acerca de la respuesta objetivo o bien el conjunto de parámetros eléctricos que la modelan, se llega a determinar los parámetros geométricos que nos permiten obtener la misma respuesta EM. Después de unas pocas iteraciones se llega a la convergencia del método, con una concordancia excelente entre la respuesta objetivo deseada y la solución final.

Este trabajo abre un campo prometedor hacia la aplicación de técnicas similares a diseños más complejos basadas en líneas metamateriales.

## AGRADECIMIENTOS

Este trabajo ha sido subvencionado por el Ministerio de Ciencia e Innovación, MICINN (España) a través de los proyectos EMET CSD2008-00066 (CONSOLIDER Ingenio 2010 Program), TEC2007-67630-C03 and TEC2007-68013-C02.

## BIBLIOGRAFÍA

- [1] V. G. Veselago. “*The electrodynamics of substances with simultaneously negative values of  $\epsilon$  and  $\mu$* ” Soviet Physics Uspekhi, 1968, pp. 509–514.
- [2] D. R. Smith, W. J. Padilla, D. C. Vier, S. C. Nemat-Nasser and Schultz. “*Composite medium with simultaneously negative permeability and permittivity*”. Physical Review letters, 2000, vol. 84, pp. 4184–4187.
- [3] J. B. Pendry, A. J. Holden, D. J. Robbins, and W. J. Stewart. “*Magnetism from conductors and enhanced non linear phenomena*”, IEEE Transactions on Microwave Theory and Techniques, 1999, vol. 47, pp. 2075-2084.
- [4] C. Caloz, T. Itoh, “*Electromagnetic Metamaterials: transmission line theory and microwave applications*”. Wiley Interscience, 2006.
- [5] J. D. Baena, J. Bonache, F. Martín, R. Marqués, E. Falcone, T. Lopetegi, M. G. Laso, J. García-García, I. Gil, M. Portillo, and M. Sorolla. “*Equivalent-circuit models for split-ring resonators and complementary split-ring resonators coupled to planar transmission lines*”, IEEE Transactions on Microwave Theory and Techniques, 2005, vol. 53, pp. 1451-1461.
- [6] F. Martín, J. Bonache, F. Falcone, M. Sorolla and R. Marqués, “*Split ring resonator-based left-handed coplanar waveguide*”. Applied Physics Letters, 2003, vol. 83, pp. 4652-4654,
- [7] F. Falcone, T. Lopetegi, M. A. G. Laso, J. D. Baena, J. Bonache, M. Beruete, R. Marqués, F. Martín and M. Sorolla. “*Babinet principle applied to the design of metasurfaces and metamaterials*”. Physical Review Letters, 2004, pp.197401–4, 2004
- [8] F. Falcone, T. Lopetegi, J. D. Baena, R. Marqués, F. Martín, and M. Sorolla, “*Effective negative stop-band microstrip lines based on complementary split ring resonators*,” IEEE Microwave Wireless Component Letters, 2004, vol. 14, no. 6, pp. 280–282.
- [9] L. J. Roglá, J. E. Rayas-Sánchez, V. E. Boria and J. Carbonell, “*EM-based space mapping optimization of left-handed coplanar waveguide filters with split ring resonators*,” IEEE-MTT International Microwave Symposium, pp. 1241– 1244, 2007.
- [10] J. W. Bandler, R. M. Biernacki, S. H. Chen, P. A. Grobelny and R. H. Hemmers, “*Space mapping technique for electromagnetic optimization*”, IEEE Transactions on Microwave Theory and Techniques, vol. 42, pp. 2536-2544, 1994
- [11] J. W. Bandler, Q. Cheng, S. A. Dakrouby, A. S. Mohamed, M. H. Bakr, K. Madsen, and J. Søndergaard, “*Space mapping: The state of the art*”, IEEE Transactions on Microwave Theory and Techniques, vol. 52, no. 1, pp. 337–361, Jan. 2004.
- [12] J. W. Bandler, R. M. Biernacki, S. H. Chen, R. H. Hemmers and K. Madsen. “*Electromagnetic optimization exploiting aggressive space mapping*”, IEEE MTT, vol. 43, pp. 2874-2882, Dec. 1995.
- [13] J. E. Rayas-Sánchez and V. Gutierrez-Ayala. “*EM-Based Monte Carlo Analysis and Yield Prediction of Microwave Circuits Using Linear-Input Neural-Output Space Mapping*”, IEEE Transactions on Microwave Theory and Techniques, vol. 54, no. 12, pp. 4528-4537, Dec. 2006.
- [14] J. Bonache, M. Gil, I. Gil, J. Garcia-García and F. Martín, “*On the electrical characteristics of complementary metamaterial resonators* , IEEE Microwave Wireless Component Letters, vol. 16, pp. 543.545, Oct. 2006.

- [15] D. M. Pozar, *Microwave Engineering*, John Wiley & Sons, 3<sup>rd</sup> ed., 2005. Ch.3
- [16] J. Bonache, M. Gil, I. Gil, J. García-García and F. Martín, “*Parametric analysis of microstrip lines loaded with complementary split ring resonators*”, *Microwave and Optical Technology Letters*, vol. 50, no. 8, pp. 2093-2095, Aug. 2008.
- [17] K. C. Gupta, R. Garg, I. Bahl and P. Bhartia, *Microstrip lines and slotlines*. Artech House, 2<sup>nd</sup> ed. Norwood, 1996.

# Automated Synthesis of Resonant-type Metamaterial Transmission Lines using Aggressive Space Mapping

Ana Rodriguez<sup>1</sup>, Jordi Selga<sup>2</sup>, Marta Gil<sup>2</sup>, Jorge Carbonell<sup>3</sup>, Vicente E. Boria<sup>1</sup>, and Ferran Martín<sup>2</sup>

<sup>1</sup> Dpto. Comunicaciones-iTEAM, <sup>3</sup>Dpto. Ing. Electrónica, Univ. Politécnica de Valencia, 46022, Spain.

<sup>2</sup>GEMMA/CIMITEC, Dept. Eng. Electrònica, Universitat Autònoma de Barcelona, Bellaterra, 08193, Spain.

E-mail: [vboria@dcom.upv.es](mailto:vboria@dcom.upv.es), [Ferran.Martin@uab.es](mailto:Ferran.Martin@uab.es)

**Abstract** — A technique for the automated generation of the layout of microstrip lines loaded with complementary split ring resonators (CSRRs) is proposed. This synthesis strategy presents a great practical interest, due to the reduction in terms of computational efforts, that is achieved without any significant lack of accuracy in the final solution. The application makes use of an aggressive space mapping (ASM) algorithm based on a constrained Broyden-based input approach. In this case, the parameter extraction (PE) does not require of any optimization, since the circuital parameters of the metamaterial transmission line can be determined following a straightforward method.

**Index Terms** — Space Mapping, Broyden, Metamaterial Transmission Lines, Complementary Split Ring Resonators.

## I. INTRODUCTION

Metamaterial transmission lines have been widely studied in the recent years, and great part of the research effort has been orientated to their synthesis [1]. Typically, these lines have smaller size than the conventional ones and provide additional control parameters, thus being considered more convenient for many practical applications. In the microwave range there are basically two ways of achieving such structures. One consists on loading standard transmission lines with series capacitances and shunt inductances (CL-loaded approach), presenting as result a composite right/left handed (CRLH) behavior [1]. The other approach, known as resonant-type, combines resonant sub-wavelength particles, such as split ring resonators (SRRs) or their complementary particles (i.e. the CSRRs), with shunt inductances or series capacitances etched on a host transmission line [2]. Both of them typically show a left-handed behavior at low frequencies, but exhibit also a right-handed transmission band at higher frequencies due to line parasitic effects. This work is focused on the resonant-type metamaterial transmission line approach, in particular on the synthesis of microstrip lines loaded with CSRRs (i.e. negative effective permittivity), which provide a stop-band response.

In the past, the synthesis of such lines has been done based on the experience of designers with the help of full-wave electromagnetic (EM) simulators and parameter extraction methods. The direct optimization of an electromagnetic model using optimization tools (nowadays available in most commercial EM simulation software) is intensive CPU demanding and it does not always work properly, due to the number of variables involved and their mutual dependence.

Hence, the interest of automating the synthesis process is high, and it can be efficiently achieved using space mapping (SM) techniques. Some of the authors of this work were pioneers in applying this kind of algorithms to the synthesis of metamaterial structures, succeeding in the design of simple coplanar waveguide filters based on SRRs [3].

After the Aggressive Space Mapping (ASM) method was originally introduced by Bandler et al. in 1995 [4], several model enhancements have been proposed in the literature. One of them is the improved constrained Broyden-based linear SM [5], which has been used in our synthesis strategy. The considered approach makes use of constrains, so unwanted solutions are not reached, thus helping to avoid instabilities of the algorithm. Too small dimensions may have an impossible implementation due to technological reasons. And on the other hand, if they are too high, the equivalent circuit model used for the PE stage might be inaccurate [6], which is critical for ASM convergence. The shrinking factor  $\delta$  has also been estimated empirically to lie between 0.3 and 0.4, as it was previously suggested in [5]. Since different types of variables are handled (physical and electrical), the classical initialization of the ASM algorithm with the identity of the Broyden matrix is not used. Instead, a numerical derivative based approach has been considered (see section III.D), which leads to get a better starting point and faster convergence.

The aim of this work is to accelerate and simplify the synthesis process of the CSRR-loaded microstrip lines, whose topology and circuit model are explained in Section II. Next, the aggressive space mapping (ASM) technique we have followed is outlined in Section III, where emphasis is made on the more specific steps of our synthesis strategy. It must be noticed that our PE stage does not require of any optimization, which is very convenient in terms of CPU time reduction. Therefore, the required effort is just related to the run of a reasonable small number of EM simulations. Our new automated synthesis technique has been successfully applied to two different examples shown in Section IV.

## II . CSRR-LOADED MICROSTRIP LINES: TOPOLOGY AND ANALYSIS TOOLS

The unit cell of a microstrip line loaded with CSRRs is depicted in Fig. 1(a), with the relevant dimensions describing the structure. As long as the electrical size of the CSRRs is

much smaller than the operating wavelength the lumped elements model, shown in Fig. 1(b), is proven to describe the response of the cell precisely [7].

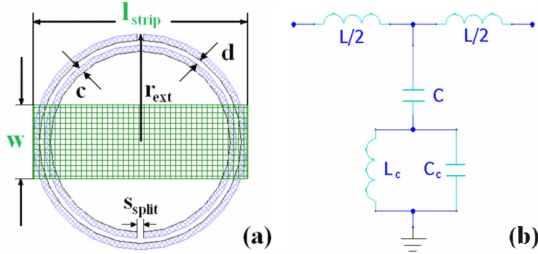


Fig. 1 Cell under study: microstrip transmission line loaded with CSRR etched in the ground plane (a), and lumped element equivalent T-circuit model (b).

In the equivalent circuit model  $L$  is the line inductance;  $C$  is the coupling capacitance between the line and the CSRRs, and the parallel tank  $C_c$  and  $L_c$  models the reactive elements of the CSRR (ohmic losses could be taken into account by including a parallel resistance in the model, see [6]). Although there are models that link the geometry of the structure to the circuit parameters, the line and the CSRR are not isolated but coupled, so such simple models cannot be straightforwardly used to find the cell topology. Nevertheless, the method proposed in [6] will be used for the PE stage of our algorithm, since it will allow a very fast and accurate determination of the equivalent circuit elements shown in Fig. 1(b).

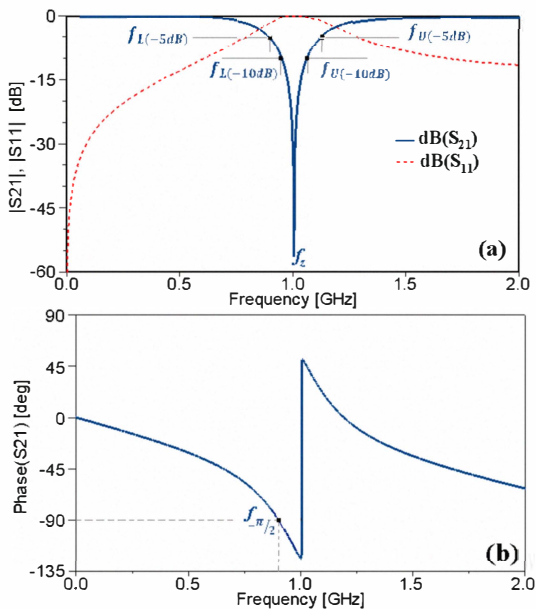


Fig. 2 EM simulated magnitude (a) and phase (b) of scattering parameters for the cell depicted in Fig 1(a), where  $w=3.85$ ,  $r_{ext}=5.65$ ,  $d=0.33$ ,  $c=s_{split}=0.25$  and  $l_{strip}=11.30$  (all dimensions in mm).

For the accurate EM modeling of the cell under study, we will make use of the commercial software Ansoft Designer, which provides the scattering parameters (see Fig. 2) without considering losses in CPU times around 90 sec. These

simulation results were obtained with a standard computer having 3GB of RAM and a 2.86GHz clock processor. On the other hand, the equivalent circuit of Fig. 1(b) will be used to provide practically immediate coarse responses.

### III. THE ASM IMPLEMENTATION

Aggressive Space Mapping is a widely recognized technique for the efficient optimization of microwave devices. Every strategy based on ASM assumes that the structure under consideration can be simulated using two models: a fine model which is complex and computationally demanding but accurate, and a coarse model that is CPU efficient but less precise [4]. Efficient optimization of the fine model (EM tool) is achieved by means of the iterative optimization of the coarse model (equivalent circuit). The ASM algorithm tries to find a mapping ( $P$ ), relating the parameters of the EM model ( $\mathbf{x}_{em}$ ) and of the coarse model ( $\mathbf{x}_c$ ):

$$\mathbf{x}_c = P(\mathbf{x}_{em}) \quad (1)$$

In our case, the electric parameters  $L$ ,  $C$ ,  $L_c$  and  $C_c$  are the elements defining the coarse model. In order to simplify the synthesis technique, not all the geometry parameters of the EM model will be considered. The chosen set of variables in  $\mathbf{x}_{em}$  are the width of the microstrip line  $w$ , the external CSRR radius  $r_{ext}$ , the width of the slots  $c$ , and the distance between them  $d$ , see Fig. 1(b). The split of the CSRR is taken as a square gap of side  $s_{split} = c$ , and the length of the line  $l_{strip}$  is fixed to the diameter of the external ring of the CSRR.

We have followed a constrained Broyden-based input SM algorithm [5], which makes use of quasi-Newton type iteration for predicting the next solution of the EM model

$$\mathbf{x}_{em}^{(j+1)} = \mathbf{x}_{em}^{(j)} + \mathbf{h} \quad (2)$$

where  $\mathbf{h}$  is the step size in the quasi-Newton direction. Using the constrained approach,  $\mathbf{h}$  will be decreased in the same quasi-Newton direction by a factor when the new vector  $\mathbf{x}_{em}$  is not within the acceptable established limits, thus letting the algorithm continue with normal evolution flow once it is adjusted. We have found empirically that the shrinking factor leading to a good convergence of the algorithm lies between 0.3 and 0.4. The ASM algorithm converges when the root of the system of non linear equations given by

$$f(\mathbf{x}_{em}) = P(\mathbf{x}_{em}) - \mathbf{x}_c^* \quad (3)$$

is found, which implies that the EM model response should approximate the optimal coarse model response  $\mathbf{x}_c^*$ .

#### A. Optimal Coarse Solution $\mathbf{x}_c^*$

The initial step in any ASM-based synthesis methodology requires to find an optimal solution of the coarse model  $\mathbf{x}_c^*$ , i.e. the electrical parameter values that define the target frequency

response to synthesize. These values can be known in advance, but if not, they must be calculated to satisfy the desired specifications. In our solution, the required specifications are: the transmission zero frequency  $f_z$  and the frequencies which define the bandwidth of the transmission response at -10dB ( $f_{L-10dB}$ ,  $f_{U-10dB}$ ) and -5dB ( $f_{L-5dB}$ ,  $f_{U-5dB}$ ), see Fig 2(a). A fixed ratio between the reactive elements  $L_c/C_c$  has been chosen in order to derive  $\mathbf{x}_c^*$ , and this ratio must be within a certain range in order to guarantee that the solutions obtained for the CSRRs are implementable [8].

Then, solving a set of nonlinear equations related to the specifications, we can easily find  $\mathbf{x}_c^*$ . Table I summarizes the values of the optimal coarse solutions used for the synthesis of the two examples considered in this paper.

TABLE I  
OPTIMAL COARSE SOLUTIONS AND TX. ZERO FREQUENCIES

	$L$ [nH]	$C$ [pF]	$L_c$ [nH]	$C_c$ [pF]	$f_z$ [GHz]
$\mathbf{x}_{cl}^*$	5.08	4.43	2.98	4.06	1
$\mathbf{x}_{c2}^*$	4.86	1.88	2.18	2.89	1.6

#### B. Estimation of $\mathbf{x}_{em}^{(j)}$

The next step consists on finding an initial geometry of the cell, i.e.  $\mathbf{x}_{em}^{(j)}$ . To obtain the microstrip line width, a classical expression for the characteristic impedance is used [9]. For the CSRR dimensions, we have employed the expressions given in [7] for characterizing this particle, but fixing one of the geometry parameters in order to find a deterministic solution.

In this first approach,  $c$  is fixed to 0.25mm, since smaller values than 0.15 mm cannot be easily manufactured, and much bigger ones would involve too big dimensions for the CSRR. As it was explained before, the length of the strip is set equal to the diameter of the CSRR. In Table II, the estimations of  $\mathbf{x}_{em}^{(j)}$  for the two considered examples are given.

TABLE II  
FIRST ESTIMATION OF PHYSICAL DIMENSIONS

	$r_{ext}$ [mm]	$c$ [mm]	$d$ [mm]	$w$ [mm]	$l_{strip}$ [mm]
$\mathbf{x}_{em1}^{(j)}$	6.39	0.25	0.95	2.43	12.78
$\mathbf{x}_{em2}^{(j)}$	4.83	0.25	0.93	1.16	9.66

#### C. Parameter Extraction Algorithm

The equation system which permits to obtain the different electrical parameters of the equivalent circuit consists on

$$f_o = \frac{1}{2\pi\sqrt{L_c C}} \quad (4)$$

$$f_z = \frac{1}{2\pi\sqrt{L_c(C+C_c)}} \quad (5)$$

$$Z_s(j\omega_{-\pi/2}) = -Z_p(j\omega_{-\pi/2}) \quad (6)$$

where the exact meaning of  $f_o$ ,  $f_z$ ,  $Z_s(j\omega)$ ,  $Z_p(j\omega)$  and  $\omega_{\pi/2}$ , and how they are related to EM simulated data, are explicitly detailed in [6]. Hence, following this approach, the corresponding  $\mathbf{x}_c$  vector is straightforwardly derived from the EM simulation results.

#### D. Initialization and Update of Broyden Matrix

To accelerate the convergence of the ASM algorithm, we have implemented a finite differences scheme to initiate the Broyden matrix. This technique is different from the common initialization approach followed in previous works which directly uses the identity matrix. The variation of each parameter of  $\mathbf{x}_c$  is simply obtained from PE corresponding to small perturbations on every component of  $\mathbf{x}_{em}^{(0)}$ . In our case, only four additional EM simulations are just needed. Then, the initial Broyden matrix can be easily estimated as follows

$$B^{(1)} = \begin{pmatrix} \frac{\partial L}{\partial w} & \frac{\partial L}{\partial r_{ext}} & \frac{\partial L}{\partial c} & \frac{\partial L}{\partial d} \\ \frac{\partial C}{\partial w} & \frac{\partial C}{\partial r_{ext}} & \frac{\partial C}{\partial c} & \frac{\partial C}{\partial d} \\ \frac{\partial L_c}{\partial w} & \frac{\partial L_c}{\partial r_{ext}} & \frac{\partial L_c}{\partial c} & \frac{\partial L_c}{\partial d} \\ \frac{\partial C_c}{\partial w} & \frac{\partial C_c}{\partial r_{ext}} & \frac{\partial C_c}{\partial c} & \frac{\partial C_c}{\partial d} \end{pmatrix} \quad (7)$$

The update of the matrix for the next iterations of the ASM algorithm responds to the classical approach [4]

$$B^{(j+1)} = B^{(j)} + \frac{f^{(j+1)} h^{(j)T}}{h^{(j)T} h^{(j)}} \quad (8)$$

This Broyden matrix is used during the ASM algorithm to obtain the new step  $\mathbf{h}$ , used to calculate the next  $\mathbf{x}_{em}$  in (2).

## IV. RESULTS

Two examples are presented in order to illustrate the efficiency and robustness of the proposed synthesis technique. In the first example, the optimal coarse solution is chosen equal to the one provided in [6], with the aim of validating our new synthesis methodology. In both examples, the selected substrate is the commercial *Rogers RO1310* with thickness  $t=1.27$ mm and dielectric constant  $\epsilon_r=10.2$ .

TABLE III LAYOUT FOUND FOR OPTIMIZED SOLUTION					
	$r_{ext}$ [mm]	$c$ [mm]	$d$ [mm]	$w$ [mm]	$l_{strip}$ [mm]
$\mathbf{x}_{em1}^*$	5.68	0.36	0.33	4.97	11.36
$\mathbf{x}_{em2}^*$	4.01	0.43	0.15	1.94	8.02

#### A. Validation Example

In the validation example, global convergence is achieved after 22 iterations, which in terms of CPU time means around 35 minutes. However, after the 10-th iteration, the error

defined as the norm of expression (3) is already small. In Fig. 3, we can see that the simulation results for the optimal coarse solution  $\mathbf{x}_e^*$  and the final layout  $\mathbf{x}_{em}^*$  exhibit a very good matching. It must be noticed that the final solution dimensions (see Table III) are very close to the ones published in [6].

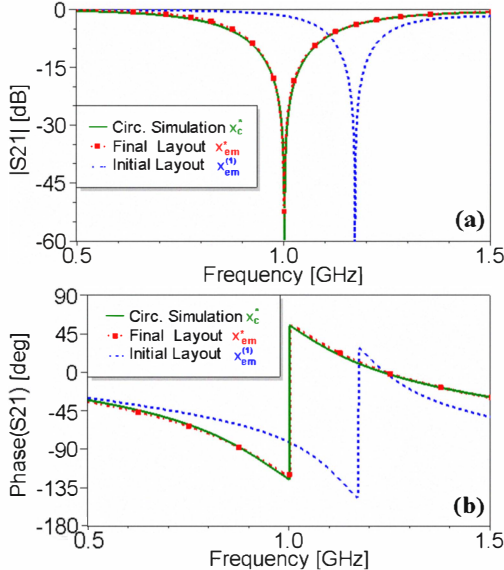


Fig. 3 Magnitude (a) and phase (b) of transmission coefficient  $S_{21}$  at initial solution  $\mathbf{x}_{em}^{(0)}$ , final solution  $\mathbf{x}_{em}^*$  and target response  $\mathbf{x}_e^*$ .

#### B. Application Example

Another example, for a different transmission zero frequency (i.e.  $f_z=1.6\text{GHz}$ ), has been considered next. The convergence is reached with a shrinking factor  $\delta=0.4$ , just after 16 iterations with a CPU effort of 20 minutes (see Fig. 4).

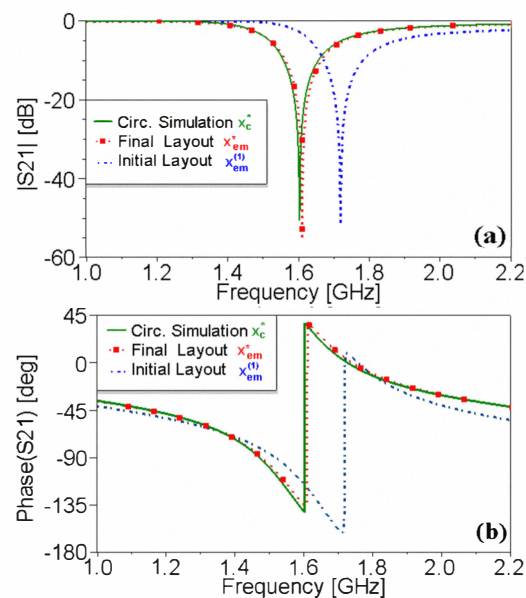


Fig. 4 Magnitude (a) and phase (b) of transmission coefficient  $S_{21}$  at initial solution  $\mathbf{x}_{em}^{(0)}$ , final solution  $\mathbf{x}_{em}^*$  and target response  $\mathbf{x}_e^*$ .

The final dimensions of the geometry can also be found in Table III. Convergence to a very similar value was also obtained with  $\delta=0.3$ , but the final error was slightly larger.

#### V. CONCLUSION

The proposed ASM technique is demonstrated to be a useful and efficient tool to synthesize the layout of CSRR-loaded microstrip lines. Convergence is reached after a few iterations with an excellent agreement between the target response and the final solution. This work opens a promising path towards the application of similar methodologies to synthesize more complex designs based on metamaterial transmission lines.

#### ACKNOWLEDGEMENT

This work has been supported by MCI (Spain) through the projects EMET CSD2008-00066 (CONSOLIDER Ingenio 2010 Program), TEC2007-67630-C03 and TEC2007-68013-C02. Special thanks are also given to Generalitat de Catalunya for funding CIMITEC and for supporting GEMMA through the project 2009SGR-421. Jordi Selga has an FPU grant (AP2008-04707) from Ministerio de Educación (Spain).

#### REFERENCES

- [1] C. Caloz and T. Itoh, *Electromagnetic Metamaterials: Transmission Line Theory and Microwave Applications*, New York: John Wiley & Sons, 2006.
- [2] R. Marqués, F. Martín and M. Sorolla, *Metamaterials with Negative Parameters: Theory, Design and Microwave Applications*, New York: John Wiley & Sons, 2007.
- [3] L. J. Roglá, J. E. Rayas-Sánchez, V. E. Boria and J. Carbonell, "EM-based space mapping optimization of left-handed coplanar waveguide filters with split ring resonators," *IEEE-MTT Int'l Microwave Symp.*, pp. 1241–1244, June 2007.
- [4] J.W. Bandler, R.M. Biernacki, S.H. Chen, R.H. Hemmers and K. Madsen "Electromagnetic optimization exploiting aggressive space mapping", *IEEE MTT*, vol. 43, pp. 2874-2882, Dec. 1995.
- [5] J.E. Rayas-Sánchez and V. Gutierrez-Ayala, "EM-Based Monte Carlo Analysis and Yield Prediction of Microwave Circuits Using Linear-Input Neural-Output Space Mapping," *IEEE MTT*, vol. 54, no. 12, pp. 4528-4537, Dec. 2006.
- [6] J. Bonache, M. Gil, I. Gil, J. García-García and F. Martín, "On the electrical characteristics of complementary metamaterial resonators," *IEEE MWCL*, vol. 16, pp. 543-545, Oct. 2006.
- [7] J.D. Baena, J. Bonache, F. Martín, R. Marqués, F. Falcone, T. Lopetegi, M.A.G. Laso, J. García, I. Gil, M. Flores and M. Sorolla, "Equivalent circuit models for split ring resonators and complementary split rings resonators coupled to planar transmission lines", *IEEE MTT*, vol. 53, pp. 1451-1461, April 2005.
- [8] J. Bonache, M. Gil, I. Gil, J. García-García and F. Martín, "Parametric analysis of microstrip lines loaded with complementary split ring resonators," *Microw. Opt. Technol. Lett.*, vol. 50, no. 8, pp. 2093-2095, Aug. 2008.
- [9] D.M. Pozar, *Microwave Engineering*, John Wiley, 2005.

# Synthesis of Planar Microwave Circuits Through Aggressive Space Mapping Using Commercially Available Software Packages

Jordi Selga,<sup>1</sup> Ana Rodríguez,<sup>2</sup> Marta Gil,<sup>1</sup> Jorge Carbonell,<sup>3</sup>  
Vicente E. Boria,<sup>2</sup> Ferran Martín<sup>1</sup>

<sup>1</sup> GEMMA/CIMITEC, Departament d'Enginyeria Electrònica, Universitat Autònoma de Barcelona, 08193 Bellaterra, Barcelona, Spain

<sup>2</sup> Departamento de Comunicaciones-iTEAM, Universidad Politécnica de Valencia, 46022 Valencia, Spain

<sup>3</sup> Departamento de Ingeniería Electrónica, Universidad Politécnica de Valencia, 46022 Valencia, Spain

Received 27 November 2009; accepted 3 May 2010

**ABSTRACT:** This article is focused on the practical implementation of a software tool for the synthesis of planar microwave circuits based on aggressive space mapping (ASM), which makes use of commercially available software packages as the core program (MATLAB<sup>®</sup>) and as the electromagnetic (EM) fine model simulation space (Agilent Momentum<sup>®</sup>). All technical details related to the control of the cited EM commercial software tool, by means of a general purpose and user-friendly environment (MATLAB in our case), are discussed in detail. The new synthesis tool has been designed to cope with the automatic layout generation of planar metamaterial structures, which is a novel practical application of the ASM algorithm. More specifically, the automated synthesis of microstrip lines loaded with complementary split ring resonators has been considered in this work. However, this synthesis tool can be easily customized to deal with the design of many other planar structures. © 2010 Wiley Periodicals, Inc. Int J RF and Microwave CAE 00:000–000, 2010.

**Keywords:** space mapping; planar microwave circuits; microstrip technology metamaterial transmission lines; complementary split ring resonator

## I. INTRODUCTION

Aggressive space mapping (ASM), originally proposed by Bandler et al. in 1995 [1], is a technique for electromagnetic (EM) optimization that uses a Newton-type iteration to find the EM solution of a given problem, provided a set of specifications, or requirements, is known. It is indeed an improved approach to space mapping (SM) (also proposed by Bandler et al. [2] in their pioneering work), where efficiency is enhanced by using each approximate solution to the problem in the iteration process, so that a progressively improved design after each iteration is expected. A recent paper on the state-of-the-art and relevant achievements of SM optimization can be found in Ref. [3]. However, to the authors' knowledge, the prac-

tical application of the ASM algorithm to the completely automated design of planar metamaterial transmission lines has not been discussed up to now.

In both SM and ASM techniques, two simulation spaces are considered. In one simulation space,  $\mathbf{X}_c$ , the variables are linked to a coarse model, which is simple and computationally efficient, although not accurate, whereas in the other space,  $\mathbf{X}_f$ , the variables are linked to a fine model, typically more complex and CPU intensive but significantly more accurate. Let us consider that the model parameters in the coarse and fine model are represented by the vectors  $\mathbf{x}_c$  and  $\mathbf{x}_f$ , respectively. The goal in ASM is to solve the following set of nonlinear equations:

$$\mathbf{f}(\mathbf{x}_f) = \mathbf{P}(\mathbf{x}_f) - \mathbf{x}_c^* = 0 \quad (1)$$

where  $\mathbf{x}_c^*$  is the vector corresponding to the parameters of the coarse model providing the target response, and  $\mathbf{P}$  is a mapping function between the coarse and fine model

Correspondence to: J. Selga; e-mail: jordi.selga@uab.cat  
DOI 10.1002/mmce.20458

Published online in Wiley InterScience (www.interscience.wiley.com).

spaces that provides the coarse model parameters from the fine model parameters (typically,  $\mathbf{x}_c$  is inferred from  $\mathbf{x}_f$  through a parameter extraction method). Let us assume that  $\mathbf{x}_f^{(j)}$  is the  $j$ -th approximation to the solution of (1) and  $\mathbf{f}^{(j)}$  is the error function corresponding to  $\mathbf{f}(\mathbf{x}_f^{(j)})$ . The next vector of the iterative process  $\mathbf{x}_f^{(j+1)}$  is found by a quasi-Newton iteration according to

$$\mathbf{x}_f^{(j+1)} = \mathbf{x}_f^{(j)} + \mathbf{h}^{(j)} \quad (2)$$

where  $\mathbf{h}^{(j)}$  is given by:

$$\mathbf{B}^{(j)} \mathbf{h}^{(j)} = -\mathbf{f}^{(j)} \quad (3)$$

and  $\mathbf{B}^{(j)}$  is an approach to the Broyden matrix [2]:

$$\mathbf{B}^{(j+1)} = \mathbf{B}^{(j)} + \frac{\mathbf{f}^{(j+1)} \mathbf{h}^{(j)T}}{\mathbf{h}^{(j)T} \mathbf{h}^{(j)}} \quad (4)$$

which is also updated at each iterative step. In (4), the superindex  $T$  stands for transpose (so that the numerator in the second term of the right-hand side of expression (4) is a matrix and the denominator is a real number).

When the two spaces deal with the same variables, typically  $\mathbf{x}_f^{(l)} = \mathbf{x}_c^*$  and  $\mathbf{B} = 1$  (the identity matrix). However, this is not always the case, as occurs in the present work. Therefore, we must clearly establish how the algorithm is initiated. In the next section, we will discuss this point and the flow diagram of the ASM algorithm, after presenting the two simulation spaces we are dealing with. In Section III, the strategy for the implementation of the ASM algorithm using two commercially available software packages (i.e., the MATLAB and the Agilent Momentum tools) will be discussed. An application example will be provided in Section IV. Finally, the main conclusions will be highlighted in Section V.

## II. COMPUTATIONAL FLOW DIAGRAM OF THE ASM ALGORITHM

In this article, we deal with the synthesis of planar microwave circuits constituted by building blocks, which can be described by means of lumped element equivalent circuit models. Hence, the considered fine and coarse models are the EM and the circuit models, respectively. The EM model provides the response of the planar circuit (typically the  $S$ -parameters) by solving the Maxwell equations. To this end, it is necessary to provide the physical parameters of the substrate (dielectric constant, loss tangent, etc.), as well as its dimensions (thicknesses of the dielectric and metallic layers), and the topology (layout) of the structure. The EM response of the circuit is typically obtained with the help of commercial tools, such as the one considered in this article, i.e., the Agilent Momentum EM software package. These tools can be very accurate but at the expense of large computation times, thus not being very efficient for design purposes. However, the electrical response of equivalent circuit models, which can be obtained by means of commercial circuit simulators almost instantaneously, can be used to adjust

the parameters of the circuit model to satisfy certain specifications or requirements. Then, the ASM technique can be used to infer the circuit layout providing the same EM response than the (target) electrical response of the circuit model. The validity of the solution in the fine (EM) model space can be confirmed by comparing the responses in both spaces, but indeed, it can also be corroborated by evaluating the error function (1) and confirming that this is smaller than a certain predefined norm.

Let us now discuss how to deal with spaces using different variables within the frame of the ASM algorithm. First of all, it is very convenient to work with the same number of variables in both spaces. In this way, the mapping function  $\mathbf{P}$  (typically modeled by means of a matrix) is directly invertible, which is very useful when solving  $\mathbf{h}$  from Eq. (3). The number of variables is determined by the number of elements of the circuit model of the structure under consideration, as well as by the number of geometry dimensions to be synthesized.

The process is started by providing a first vector in the fine model space,  $\mathbf{x}_f^{(1)}$ , whose elements are parameters determining the geometry of the structure. To this end, we can make use of existing analytical, empirical or numerical models of the structure (or of its constitutive building blocks) that link the circuit parameters to the geometrical and substrate parameters. The next step is the calculation of  $\mathbf{P}(\mathbf{x}_f^{(1)})$ , which is the first candidate vector in the coarse space. This vector, containing a set of circuit elements, is inferred through some parameter extraction procedure (for which it is necessary to infer previously the response of  $\mathbf{x}_f^{(1)}$  in the fine model space). With this coarse vector, we can evaluate the error function at the first iteration,  $\mathbf{f}(\mathbf{x}_f^{(1)}) = \mathbf{f}^{(1)}$ . Once the first error function is known, we need a first candidate for the Broyden matrix,  $\mathbf{B}^{(1)}$ , to obtain  $\mathbf{h}^{(1)}$  from (3). With  $\mathbf{h}^{(1)}$  and  $\mathbf{x}_f^{(1)}$  we can calculate  $\mathbf{x}_f^{(2)}$  from (2), and the process is iterated until convergence is achieved.

Let us denote the variables in the fine and coarse model spaces as  $x_{f1}, x_{f2}, \dots, x_{fm}$ , and  $x_{c1}, x_{c2}, \dots, x_{cm}$ , respectively, where  $m$  is the dimension of the vectors in both spaces. The first Broyden matrix  $\mathbf{B}^{(1)}$  is initiated as follows:

$$\begin{pmatrix} \frac{\partial x_{c1}}{\partial x_{f1}} & \frac{\partial x_{c1}}{\partial x_{f2}} & \dots & \frac{\partial x_{c1}}{\partial x_{fm}} \\ \frac{\partial x_{c2}}{\partial x_{f1}} & \frac{\partial x_{c2}}{\partial x_{f2}} & \dots & \frac{\partial x_{c2}}{\partial x_{fm}} \\ \vdots & \vdots & \dots & \vdots \\ \frac{\partial x_{cm}}{\partial x_{f1}} & \frac{\partial x_{cm}}{\partial x_{f2}} & \dots & \frac{\partial x_{cm}}{\partial x_{fm}} \end{pmatrix} \quad (5)$$

where the derivatives are obtained from the variation of the coarse model parameters,  $\delta x_{ci}$ , that result after introducing a small perturbation of the parameters in the fine model,  $\delta x_{fi}$  (the parameter extraction must be applied  $m$  additional times). The flow chart of the implemented ASM algorithm is depicted in Figure 1. It is finished when the norm of the error function  $|\mathbf{f}(\mathbf{x}_f)|$  is smaller than a certain predefined value,  $\eta$ .

## III. IMPLEMENTATION OF THE ASM ALGORITHM BY MEANS OF MATLAB AND MOMENTUM SOFTWARE PACKAGES

An original contribution of this work is that the iterative ASM procedure is completely automated and controlled

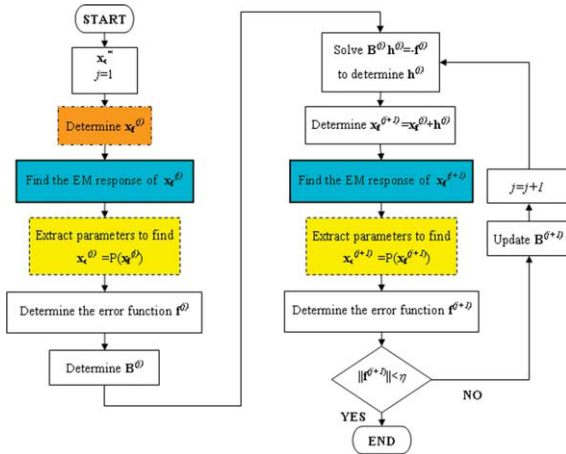


**Figure 1** Flow chart of the ASM algorithm. The stages corresponding to the initial geometry calculator, EM solver, and parameter extractor modules are indicated in dashed-dotted, solid, and dashed lines, respectively. [Color figure can be viewed in the online issue, which is available at [www.interscience.wiley.com](http://www.interscience.wiley.com).]

from the MATLAB commercial software, which acts as the core program of the implemented algorithm. There are three main building blocks in the program: (i) a module for the determination of the initial geometry of the structure,  $x_f^{(1)}$ , from the target circuit parameters,  $x_c^*$ ; (ii) an EM solver (in our case linked to the Agilent Momentum commercial software); and (iii) a module for parameter extraction. From now on, let us identify these modules with the following terms: initial geometry calculator, EM solver, and parameter extractor, respectively. The initial geometry calculator is only used at the beginning of the algorithm to determine  $x_f^{(1)}$ . It provides a set of geometrical parameters from the target coarse (circuit) model parameters and existing models linking the variables of both spaces. The EM solver computes the *S*-parameters of the structure from the physical parameters (and geometry) of the substrate and a given set of fine model parameters ( $x_f$ ), that is, the geometrical parameters that univocally determine the layout of the structure. The parameter extractor uses the EM response given by the full-wave commercial solver and produces a set of circuit parameters ( $x_c$ ) whose electrical response is very similar to the EM response of the structure (it is assumed that the circuit models describe correctly the behavior of the considered structures, at least in the frequency range of interest). Contrary to the initial geometry calculator, the EM solver and the parameter extractor modules are active at each iterative step.

Obviously, the details of the previously cited modules depend on the particular structures under consideration, and this aspect will be discussed in the next section. However, there is an important aspect that does not depend on the type of structures that we want to synthesize: the control of the full-wave EM solver Agilent Momentum by means of the MATLAB commercial software. The input of the EM solver is the vector in the  $X_f$  space,  $x_f$ , containing the information relative to the geometry (layout) of the structure. From this vector, a text file equivalent to that one generated by the Agi-

lent Momentum after defining the same geometry from its computer-aided design (CAD) tool is created. Apart from this file, three additional text files are generated by the Agilent Momentum to perform an EM simulation: a text file with information related to the frequency range and number of frequency points (we consider adaptive-type simulation rather than linear), a text file defining the mesh of the structure, and a text file with the physical and geometrical parameters of the substrate. As for the geometry of the structure, such additional files are also generated by the MATLAB core program. The next step is to execute the Agilent Momentum EM simulator from MATLAB. To this end, the corresponding instruction must be added to the core program. The Agilent Momentum simulator generates a file containing the results of the EM analysis (*S*-parameters). This file is then converted to a text file and it is exported to MATLAB, this being the result of the EM solver module.

The actions carried out by the different modules of the implemented ASM algorithm are indicated by different colors in the flow chart of Figure 1.

#### IV. APPLICATION OF THE ASM ALGORITHM TO THE SYNTHESIS OF MICROSTRIP LINES LOADED WITH COMPLEMENTARY SPLIT RING RESONATORS

In this section, the described tool is applied to the synthesis of a microstrip line with a complementary split ring resonator (CSRR) [4] etched in the ground plane (see Fig. 2a). This structure is the unit cell for the design of one-dimensional structures exhibiting a negative value of the effective permittivity [4, 5]. They can also be used as building blocks for the design of stop band filters [6]. However, the main reason for choosing a CSRR-loaded microstrip transmission line as the first case study for the application of the implemented ASM algorithm is the relative complexity associated with the synthesis of these structures, where distributed and semi-lumped elements (CSRRs) are combined. The lumped element equivalent circuit model of the CSRR-loaded microstrip line is depicted in Figure 2b [7]. In this model,  $L$  is the inductance of the line,  $C$  accounts for the capacitance between the upper metallic strip (line) and the metallic region inside the CSRR, whereas  $L_c$  and  $C_c$  account for the inductance and capacitance of the CSRR. These elements are the coarse model parameters. Although seven geometrical parameters are necessary to define the layout of the structure (see Fig. 2a), we will consider from now on that the microstrip line length is twice the external radius of the CSRR,  $l = 2r_{\text{ext}}$ . Moreover, split dimensions are taken as  $s_{\text{ext}} = 0.07r_{\text{ext}}$  for the external ring and  $s_{\text{int}} = 0.07(r_{\text{ext}} - c - d)$  for the internal ring. This corresponds, approximately, to a gap aperture of 4° for each ring. In that way, the considered geometrical parameters are reduced to four:  $c$ ,  $d$ ,  $r_{\text{ext}}$ , and  $W$  (these are the variables of the fine model). The validity of the model of Figure 2b is subject to two conditions: (i) the CSRR must be electrically small and (ii) the microstrip line must not extend much beyond the limits of the CSRR (so that parasitic transmission line effects are precluded). For this last reason, we have forced  $l = 2r_{\text{ext}}$ .

Let us now focus on the details of the different modules taking into account the particular structure under

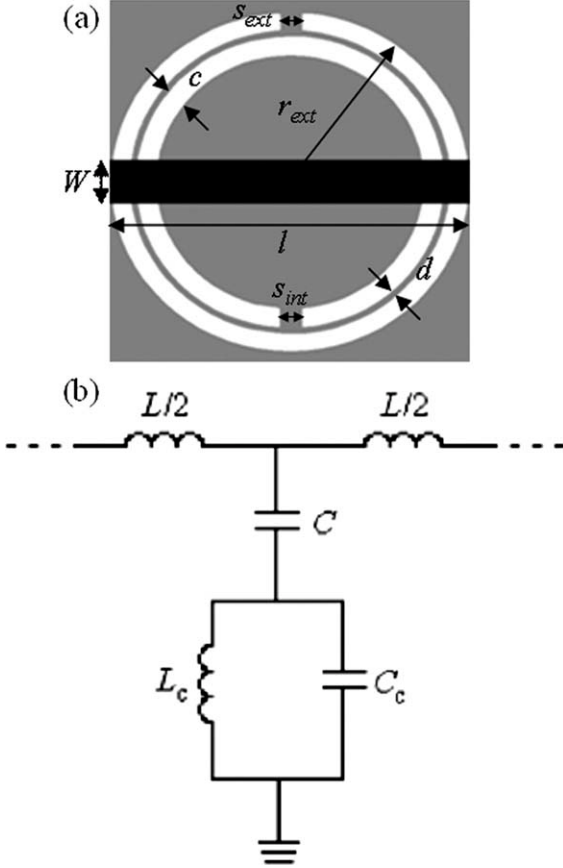


**Figure 2** Typical topology (unit cell) of a CSRR-loaded microstrip line (a) and equivalent T-circuit model (b). The relevant geometrical parameters of the structure are indicated.

consideration. Concerning the module for the determination of the initial geometry (initial geometry calculator), the analytical model for a microstrip structure [8] and the CSRR model reported in Ref. [7] have been used. Specifically, from the values of  $C$  and  $L$ , we infer the characteristic impedance of the host line [ $Z_0 = (L/C)^{1/2}$ ], and from well-known formulas [8], we determine the width of the line corresponding to this impedance value:

$$\frac{W}{h} = \begin{cases} \frac{8e^A}{e^{2A}-2} & \text{for } W/h < 2 \\ \frac{2}{\pi} \left[ B - 1 - \ln(2B-1) \right. \\ \left. + \frac{\varepsilon_r-1}{2\varepsilon_r} \left\{ \ln(B-1) + 0.39 - \frac{0.61}{\varepsilon_r} \right\} \right] & \text{for } W/h > 2 \end{cases} \quad (6)$$

where

$$A = \frac{Z_0}{60} \sqrt{\frac{\varepsilon_r+1}{2}} + \frac{\varepsilon_r-1}{\varepsilon_r+1} \left( 0.23 + \frac{0.11}{\varepsilon_r} \right) \quad (7)$$

$$B = \frac{377\pi}{2Z_0\sqrt{\varepsilon_r}}. \quad (8)$$

and  $\varepsilon_r$  and  $h$  are the dielectric constant and thickness of the substrate, respectively. Obviously, from the values of  $L$  and

$C$ , the length of the host line can also be determined. However, as we are considering that  $l = 2r_{ext}$ , the length of the host line for the first layout candidate is determined after the CSRR dimensions are obtained. To determine the CSRR dimensions, we fix the value of the rings width to a reasonable value, namely,  $c = 0.25$  mm, and from the values of  $C_c$  and  $L_c$ , we can univocally determine  $r_{ext}$  and  $d$ . To this end, the model reported in Ref. [7] has been used. Actually, the model provides the reactive elements of the CSRR from its geometry, so that we have swept  $d$  and  $r_{ext}$  (driven through an optimization algorithm) until the required values of  $C_c$  and  $L_c$  are found. This is, however, very fast since only two design parameters are involved in the optimization process. The capacitance  $C_c$  is given by expression (1) in Ref. [7], whereas the inductance  $L_c = L_o/4$ , where  $L_o$  is the inductance corresponding to a circular coplanar waveguide (CPW) structure of length  $2\pi r_o$ , strip width  $d$ , and slot width  $c$  (the detailed formula is given in Ref. [9]).

With regard to the EM solver module, the topology of the strip line (upper metal layer) is provided by giving the rectangle vertices. The topology of CSRR (lower metal layer) has been generated from polar to Cartesian coordinate transformation, and the circumferences defining the perimeter of the rings are actually 180-side polygons. With these points, the EM solver creates a suitable text file containing the layout information, which can be interpreted by Agilent Momentum. Using this file and those containing the information relative to the frequency range, mesh, and physical parameters of the substrate, the EM full-wave simulation is performed.

Finally, the parameter extractor module uses the results of the EM solver to obtain the parameters of the circuit model of Figure 2b. These parameters are inferred from the EM-simulated  $S$ -parameters according to the procedure described in Ref. [10], where three singular frequencies must be identified: (i) the transmission zero frequency,  $f_z$ ,

$$f_z = \frac{1}{2\pi\sqrt{L_c(C+C_c)}} \quad (9)$$

where the impedance of the shunt branch of the circuit model nulls; (ii) the frequency that opens the shunt branch,  $f_o$ ,

$$f_o = \frac{1}{2\pi\sqrt{L_cC_c}} \quad (10)$$

where  $S_{11}$  intercepts the unit resistance circle in the Smith Chart (this frequency is the resonance frequency of the CSRRs); and (iii) the frequency providing  $-90^\circ$  phase shift for  $S_{21}$  ( $f_{-\pi/2} = \omega_{-\pi/2}/2\pi$ ), where the series and shunt impedances of the circuit model satisfy [10]:

$$Z_s(\omega_{-\pi/2}) = -Z_p(\omega_{-\pi/2}) \quad (11)$$

As we have mentioned, at the frequency where  $S_{11}$  intercepts the unit resistance circle in the Smith Chart, the shunt branch opens and hence, the impedance of the circuit model,  $Z(f_o)$ , can be written as:

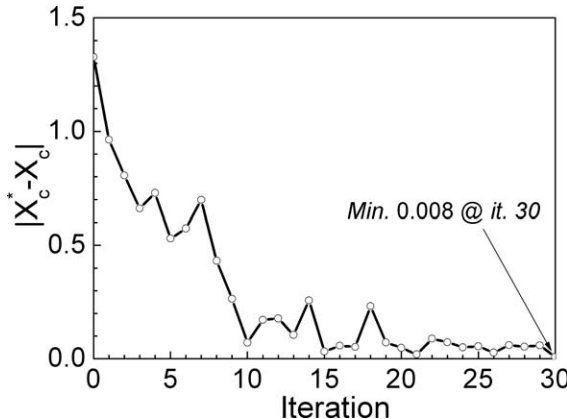


**Figure 3** Evolution of the error function for the example considered.

$$Z(f_0) = Z_0 + 2\pi L f_0 j \quad (12)$$

$Z_0$  being the reference impedance of the ports ( $Z_0 = 50 \Omega$ ).

Equations (9)–(12) are the four required conditions to determine the parameters of the circuit model. The S-parameters generated by Agilent Momentum are exported to MATLAB, where the frequencies  $f_z$ ,  $f_0$ ,  $f_{-\pi/2}$ , and the impedance  $Z(f_0)$  are identified, and then eqs. (9)–(12) are solved.

To demonstrate the viability of the ASM-based algorithm for the automated synthesis of CSRR-loaded lines, an application example is provided. The target parameters in the circuit (coarse) model are:  $L^* = 6.00 \text{ nH}$ ,  $C^* = 1.815 \text{ pF}$ ,  $L_c^* = 2.00 \text{ nH}$ , and  $C_c^* = 3.00 \text{ pF}$  (we assume that the circuit response with these parameters is the desired frequency response of the CSRR-loaded line). With these target parameters,  $f_z = 1.622 \text{ GHz}$ ,  $f_0 = 2.055 \text{ GHz}$ , and  $f_{-\pi/2} = 1.427 \text{ GHz}$ . Starting with these element values, the algorithm has been applied until the error function, calculated as follows:

$$\begin{aligned} \|\mathbf{f}(\mathbf{x}_t)\| &= |\mathbf{x}_c^* - \mathbf{x}_c| \\ &= \sqrt{(L^* - L)^2 + (C^* - C)^2 + (L_c^* - L_c)^2 + (C_c^* - C_c)^2} \end{aligned} \quad (13)$$

has been found to be smaller than  $\eta = 0.01$ , with the inductive values given in nH and the capacitance ones in pF. In the considered case, convergence has been achieved after 30 iterations (the evolution of the norm evaluated by expression (13) is depicted in Figure 3, where it can be seen a global exponential decay showing a very good convergence rate, even though some small increases due to the gradient-based iterative algorithm are present).

The target layout is depicted in Figure 4 (dimensions are:  $r_{\text{ext}} = 4.61 \text{ mm}$ ,  $d = 0.56 \text{ mm}$ ,  $W = 2.24 \text{ mm}$ , and  $c = 0.25 \text{ mm}$ , and the considered substrate is the Rogers RO3010 substrate with dielectric constant  $\epsilon_r = 10.2$  and thickness  $h = 1.27 \text{ mm}$ ), whereas the target response (i.e., the circuit simulation by considering the target circuit parameters), the EM simulation of the layout of Figure 4, and the EM simulation at iterations 4, 7, and 15 are

depicted in Figure 5. The resulting circuit parameters after convergence ( $L = 6.01 \text{ nH}$ ,  $C = 1.80 \text{ pF}$ ,  $L_c = 2.02 \text{ nH}$ , and  $C_c = 2.98 \text{ pF}$ ) are very close to the target parameters. Also, the EM simulation of the final layout is in very good agreement with the target circuit simulation in the region of interest, namely, in the vicinity of CSRR resonance (where the circuit model is valid), and it can be appreciated in Figure 5 that the intermediate responses progressively evolve to the final response.

The disagreement in the low-frequency region of  $S_{11}$  is not appreciable in a linear scale, and is caused by the fact that the image impedance of the cell corresponding to the target circuit parameters varies very slightly in the vicinity of the port impedance ( $50 \Omega$ ). Such impedance is exactly  $50 \Omega$  at the reflection zero frequency, which is very sensitive to the variation of the circuit parameters. As the parameter extraction is based on singular frequencies in the vicinity of the transmission zero frequency, it is not surprising that the EM simulation of the final layout might exhibit some deviation from the circuit model at lower frequencies. Nevertheless, in a linear scale, the agreement is very good, and it is excellent in the region of interest. At higher frequencies, the discrepancies are due to the fact that the CSRR cannot be considered to be electrically small and the circuit model starts to fail.

## V. CONCLUSIONS

In conclusion, it has been demonstrated that the commercial software tools MATLAB and Agilent Momentum can be combined for the implementation of an automated layout generation algorithm based on ASM, which is extremely useful

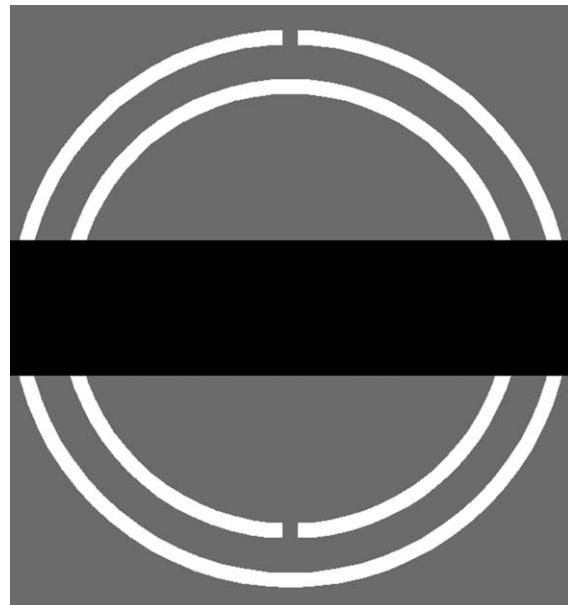


**Figure 4** Final layout of the CSRR-loaded structure. Dimensions are:  $r_{\text{ext}} = 4.61 \text{ mm}$ ,  $d = 0.56 \text{ mm}$ ,  $W = 2.24 \text{ mm}$ , and  $c = 0.25 \text{ mm}$ . The considered substrate is the Rogers RO3010 substrate with dielectric constant  $\epsilon_r = 10.2$ , thickness  $h = 1.27 \text{ mm}$  (dielectric and ohmic losses have not been taken into account).

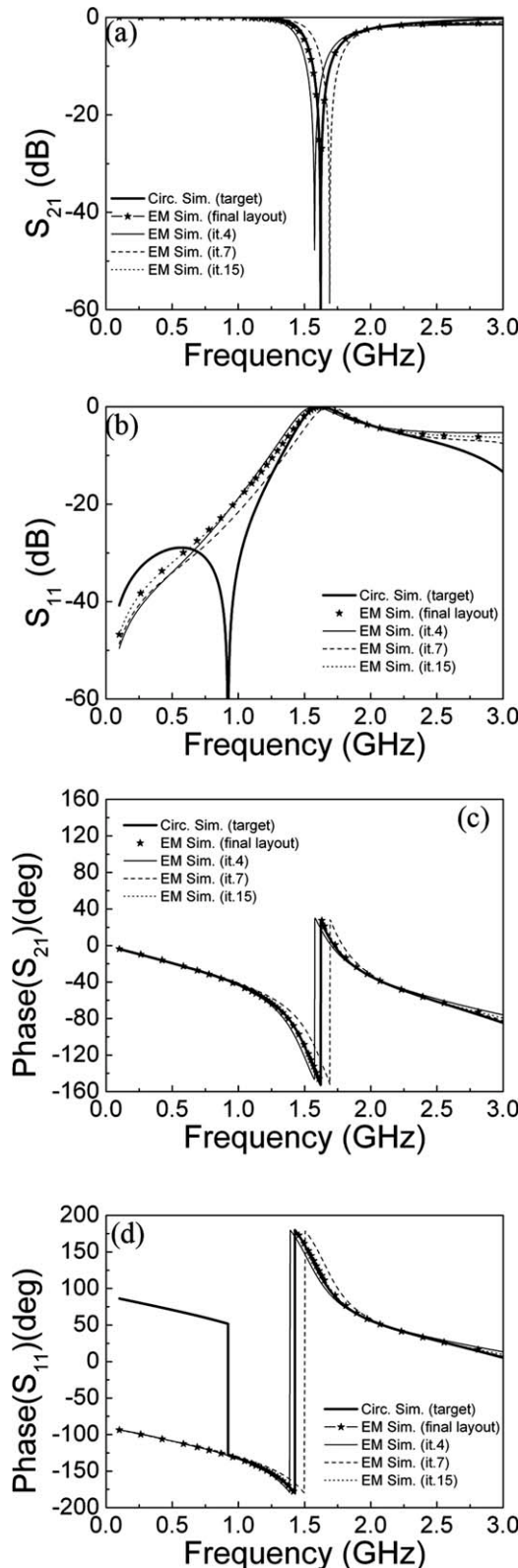


**Figure 5** Target frequency response for the structure of the considered example (obtained from circuit simulation of the model of Fig. 1 with the target parameters), and EM simulation at the indicated iteration steps, and after convergence. (a) Insertion losses; (b) return losses; (c) phase of  $S_{21}$ ; and (d) phase of  $S_{11}$ .

for the practical design of planar microwave circuits. The main details of the algorithm, containing three basic modules (the initial geometry calculator, the EM solver, and the parameter extractor) have been provided and discussed. In this work, the algorithm has been successfully validated through the synthesis of a microstrip line loaded with CSRRs. It has been found that convergence is achieved after a small number of iterations. The technique can be extended to other planar circuits, and it can be also implemented by combining MATLAB with other EM simulators (for instance, the authors have already verified this using the EM tool Ansoft Designer).

#### ACKNOWLEDGMENT

This work has been supported by MEC (Spain) through the projects TEC2007-68013-C02 METAINNOVA and TEC2007-67630-C03 CABESERES, as well as by MICINN (Spain) through the project EMET CSD2008-00066 of the CONSOLIDER Ingenio 2010 Program. Special thanks are also given to Generalitat de Catalunya for funding CIMITEC and for supporting GEMMA through the project 2009SGR-421. The Ministerio de Education (Spain) has given an FPU grant to Jordi Selga with reference AP2008-04707.

#### REFERENCES

1. J.W. Bandler, R.M. Biernacki, S.H. Chen, R.H. Hemmers, and K. Madsen, Electromagnetic optimization exploiting aggressive space mapping, *IEEE Trans Microwave Theory Tech* 43 (1995), 2874–2882.
2. J.W. Bandler, R.M. Biernacki, S.H. Chen, P.A. Grobelny, and R.H. Hemmers, Space mapping technique for electromagnetic optimization, *IEEE Trans Microwave Theory Tech* 42 (1994), 2536–2544.
3. S. Koziel, Q.S. Cheng, and J.W. Bandler, Space mapping, *IEEE Microwave Mag* 9 (2008), 105–122.
4. F. Falcone, T. Lopetegi, J.D. Baena, R. Marqués, F. Martín, and M. Sorolla, Effective negative- $\epsilon$  stop-band microstrip lines based on complementary split ring resonators, *IEEE Microwave Wireless Compon Lett* 14 (2004), 280–282.
5. F. Falcone, T. Lopetegi, M.A.G. Laso, J.D. Baena, J. Bonache, R. Marqués, F. Martín, and M. Sorolla, Babinet principle applied to the design of metasurfaces and metamaterials, *Phys Rev Lett* 93 (2004), 197401.
6. J. García-García, F. Martín, F. Falcone, J. Bonache, J.D. Baena, I. Gil, E. Amat, T. Lopetegi, M.A.G. Laso, J.A. Martoregui, M. Sorolla, and R. Marqués, Microwave filters with improved stop band based on sub-wavelength resonators, *IEEE Trans Microwave Theory Tech* 53 (2005), 1997–2006.
7. J.D. Baena, J. Bonache, F. Martín, R. Marqués, F. Falcone, T. Lopetegi, M.A.G. Laso, J. García, I. Gil, M. Flores-Portillo, and M. Sorolla, Equivalent circuit models for split ring resonators and complementary split rings resonators coupled to planar transmission lines, *IEEE Trans Microwave Theory Tech* 53 (2005), 1451–1461.
8. D.M. Pozar, *Microwave engineering*, 2nd ed., John Wiley & Sons, Inc., New York, 1998.
9. I. Bahl and P. Bhartia, *Microwave solid state circuit design*, Wiley, Toronto, ON, Canada, 1988.
10. J. Bonache, M. Gil, I. Gil, J. García-García, and F. Martín, On the electrical characteristics of complementary metamaterial resonators, *IEEE Microwave Wireless Compon Lett* 16 (2006), 543–545.

---

BIOGRAPHIES

**Jordi Selga** was born in Barcelona, Spain, in 1982. He received the Telecommunications Engineering Diploma, specializing in electronics, in 2006 and the Electronics Engineering degree in 2008 from the Universitat Autònoma de Barcelona, Barcelona, Spain. He is currently working toward his Ph.D. degree in subjects related to metamaterials and microwave circuits in the Universitat Autònoma de Barcelona. He is presently holder of a national research fellowship from the Formación de Profesorado Universitario Program of the Education and Science (Reference AP2008-4707) presented by Spanish Government (MEC).



**Ana Rodríguez** was born in Lugo, Spain. She received her Master's degree in Telecommunications Engineering at the Universidad de Vigo in 2008. As a student, she participated in the Erasmus exchange program to do her Master Thesis in Metamaterials at the University of Oulu, Finland. She has been with the Institute of Telecommunications and Multimedia Application (iTEAM) in Valencia since 2008. Currently she combines her research in iTEAM with the realization of "Master en Tecnología, Sistemas y Redes de Comunicaciones." Her main research interests are: Metamaterials and CAD design of microwave devices.



**Marta Gil** was born in Valdepeñas (Ciudad Real), Spain, in 1981. She received the degree in Physics from the Universidad de Granada in 2005 and the Ph.D. degree in Electronics Engineering from the Universitat Autònoma de Barcelona in 2009. She studied during 1 year in the Friedrich Schiller Universität Jena, in Jena, Germany. She was holder of a national research fellowship from the FPU Programm of the Education and Science Spanish Ministry (MEC) (Reference AP2005-4523). She is currently working as a researcher of the national subprogram Juan de La Cierva (JCI-2009-04502) in the Universidad de Castilla-La Mancha. Her interests include microwave engineering, metamaterials, and piezoelectric MEMS for sensing applications.



**Jorge Carbonell** was born in Valencia (Spain) in 1971. He received the M.Sc. degree in Telecommunications Engineering from the Universidad Politécnica de Valencia (Spain) in 1995 and the Ph.D. degree in Electrical Engineering, European Label with Honors, from the University of Lille (France) in 1998. From 1996 to 1998, he was with the Institut d'Electronique et de Microélectronique du Nord (IEMN) at the University of Lille (France), where his research activity included EM analysis of active and passive devices for space applications and, in particular, photonic bandgap materials. From 1999 to 2003, he worked within the wireless industry with Ericsson, Siemens, Retevisión Móvil, and Telefónica Móviles. During that period, he was involved in the design and deployment of second-generation and third-generation wireless communication systems and networks and mainly focused on radio engineering. Since January 2004, he holds a research position at the Universidad Politécnica de Valencia (Spain). His current research activity concerns the analysis and design of passive periodic structures and metamaterials.



**Vicente E. Boria** (S'91-A'99-SM'02) was born in Valencia, Spain, on May 18, 1970. He received his "Ingeniero de Telecomunicación" degree (with first-class honors) and the "Doctor Ingeniero de Telecomunicación" degree from the Universidad Politécnica de Valencia, Valencia, Spain, in 1993 and 1997, respectively. In 1993, he joined the "Departamento de Comunicaciones", Universidad Politécnica de Valencia, where he has been Full Professor since 2003. In 1995 and 1996, he was holding a Spanish Trainee position with the European Space Research and Technology Centre, European Space Agency (ESTEC-ESA), Noordwijk, The Netherlands, where he was involved in the area of EM analysis and design of passive waveguide devices. He has authored or coauthored seven chapters in technical textbooks, 65 papers in refereed international technical journals, and over 150 papers in international conference proceedings. His current research interests are focused on the analysis and automated design of passive components, left-handed and periodic structures, as well as on the simulation and measurement of power effects in passive waveguide systems. Dr. Boria has been a member of the IEEE Microwave Theory and Techniques Society (IEEE MTT-S) and the IEEE Antennas and Propagation Society (IEEE AP-S) since 1992. He

is a member of the Editorial Boards of the IEEE Transactions on Microwave Theory and Techniques, IEEE Microwave and Wireless Components Letters, Proceeding of the IET (Microwaves, Antennas, and Propagation), IET Electronics Letters, and Radio Science. He is also a member of the Technical Committees of the IEEE-MTT International Microwave Symposium and of the European Microwave Conference.



**Ferran Martín** was born in Barakaldo (Vizcaya), Spain, in 1965. He received the B.S. degree in physics and the Ph.D. degree from the Universitat Autònoma de Barcelona (UAB), Barcelona, Spain, in 1988 and 1992, respectively. From 1994 to 2006, he was an Associate Professor in Electronics in the Departament d'Enginyeria Electrònica (Universitat Autònoma de Barcelona), and since 2007, he has been a Full Professor of Electronics. In recent years, he has been involved in different research activities including modeling and simulation of electron devices for high-frequency applications, millimeter-wave and THz generation systems, and the application of electromagnetic bandgaps

to microwave and millimeter-wave circuits. He is now very active in the field of metamaterials and their application to the miniaturization and optimization of microwave circuits and antennas. He is the head of the Microwave and Millimeter Wave Engineering Group (GEMMA Group) at UAB, and director of CIMITEC, a research Center on Metamaterials supported by TECNIO (Generalitat de Catalunya). He has acted as Guest Editor for three Special Issues on metamaterials in three international journals. He has authored and coauthored over 300 technical conference, letter, and journal papers, and he is coauthor of the monograph on metamaterials entitled *Metamaterials with Negative Parameters: Theory, Design, and Microwave Applications* (Wiley, 2008). He has filed several patents on metamaterials and has headed several development contracts. Prof. Martin has organized several international events related to metamaterials, including Workshops at the IEEE International Microwave Symposium (years 2005 and 2007) and European Microwave Conference (2009). Among his distinctions, he received the 2006 Duran Farell Prize for Technological Research, he holds the Parc de Recerca UAB—Santander Technology Transfer Chair, and he has been the recipient of an ICREA ACADEMIA Award.

Published in IET Microwaves, Antennas & Propagation  
Received on 12th November 2009  
Revised on 5th March 2010  
doi: 10.1049/iet-map.2009.0551

In Special Issue on Microwave Metamaterials: Application to Devices, Circuits and Antennas



ISSN 1751-8725

# Towards the automatic layout synthesis in resonant-type metamaterial transmission lines

J. Selga<sup>1</sup> A. Rodríguez<sup>2</sup> M. Gil<sup>1</sup> J. Carbonell<sup>3</sup>  
V.E. Boria<sup>2</sup> F. Martín<sup>1</sup>

<sup>1</sup>GEMMA/CIMITEC, Departament d'Enginyeria Electrònica, Universitat Autònoma de Barcelona, 08193, Bellaterra (Barcelona), Spain

<sup>2</sup>Departamento de Comunicaciones-iTEAM, Universidad Politécnica de Valencia, 46022 Valencia, Spain

<sup>3</sup>Departamento de Ingeniería Electrónica, Universidad Politécnica de Valencia, 46022 Valencia, Spain

E-mail: jordi.selga@uab.cat

**Abstract:** The first approach towards the automatic layout generation of resonant-type metamaterial transmission lines by using space mapping optimisation is reported. Specifically, the so-called aggressive space mapping (ASM) technique is applied for synthesising microstrip lines loaded with complementary split ring resonators (CSRRs). From a certain set of elements of the circuit model of the unit cell of such lines (which is typically derived from system specifications), the topology (layout) of the CSRR-loaded microstrip line, providing the same electromagnetic response as the circuit model (within certain error limits), is generated automatically. This synthesis technique is of paramount importance for the design of metamaterial-based (or inspired) circuits implemented by means of electrically small resonators such as CSRRs and SRRs. Although the reported technique is applied here to the synthesis of a negative permittivity structure (CSRR-loaded line), the basics towards the extension of the technique to other artificial transmission lines are clearly established.

## 1 Introduction

Artificial transmission lines based on metamaterial concepts or metamaterial transmission lines have been a subject of intensive research in recent years [1–3]. These structures consist of a host line loaded with reactive elements. Owing to the presence of such reactive elements, it is possible to further control line parameters (e.g. characteristic impedance and electrical length), compared with conventional lines. Typically, metamaterial transmission lines can be implemented either by loading a host line with shunt inductors and series capacitors (CL-loaded approach) [4–6] or by etching electrically small resonators close to the line (resonant-type approach). In the latter category, metamaterial transmission lines have been implemented by loading a coplanar waveguide (CPW) with split ring resonators (SRRs) [7] and shunt-connected strips (acting as inductors) [8] or by loading a microstrip line with complementary SRRs (CSRRs) [9] and gap (or interdigital) capacitances in series configuration [10]. As CL-loaded lines, resonant-type

metamaterial transmission lines exhibit a composite right/left-handed (CRLH) behaviour, that is, they exhibit left-handed (or backward) wave propagation at low frequencies and right-handed (or forward) wave propagation at higher frequencies [11, 12]. These two bands can be merged into a single one, with a continuous transition between the backward and forward bands, by balancing the line, namely, by designing the structure so that the change in the sign of the series and shunt impedance (of the equivalent T- or  $\pi$ -circuit model) occurs at the same frequency. Such balanced structures thus exhibit a band-pass behaviour that has been used in the implementation of compact band-pass filters [13, 14] (other filters based on unbalanced lines – including non-periodic structures as well – implemented by means of electrically small resonators have also been reported [15–21]). Alternatively, it is possible to design stop band structures based on metamaterial transmission lines. This can be performed by merely loading a host line either with SRRs [22] or with CSRRs [23]. In the vicinity of the

resonance frequency of the loading resonators, the injected power is reflected back to the source, and a transmission zero is clearly visible in the frequency response. This stop band response of these lines can also be explained in terms of effective medium theory; that is, a host line loaded with a periodic array of SRRs, or CSRRs, can be seen as a one-dimensional metamaterial exhibiting a negative effective permeability and permittivity, respectively, in the vicinity of SRR, or CSRR, resonance [3, 24].

The present paper is focused on the synthesis of microstrip lines simply loaded with CSRRs (i.e. negative permittivity lines). These lines are simpler than the CRLH lines based on such resonant elements because the series gap is absent, and for this reason, the authors have chosen these lines as a first case study for the automatic generation of their layouts on the basis of space mapping optimisation [25, 26]. To the authors' knowledge, few reports about the use of space mapping techniques for the automated synthesis of metamaterial-based circuits can be found in the technical literature (for instance, see [27], in which the optimised design of simple CPW filters based on SRRs was pioneered). In the present work, a more robust technique for the automated design of negative permittivity microstrip transmission lines (acting as stop band structures) is proposed. This technique, which is implemented in a single-stage space mapping optimisation (as opposite to [27]) and uses a reliable and accurate parameter extraction algorithm, can be easily extended to the synthesis of CRLH lines (based on both CSRRs and SRRs) and to more complex structures based on metamaterial concepts.

The paper is organised as follows. In Section 2, we will consider in detail the typical topology and circuit model of CSRR-loaded lines. In Section 3, the aggressive space mapping (ASM) technique will be explained, and we will discuss the particular strategies for the synthesis of the proposed structures. Some application examples will be given in Section 4. Finally, the main concluding remarks will be highlighted in Section 5.

## 2 CSRR-loaded microstrip lines: topology, circuit model and parameter extraction

The typical topology (unit cell) of a CSRR-loaded microstrip line is depicted in Fig. 1a. It consists of a microstrip line with a CSRR etched in the ground plane beneath the conductor strip. The equivalent T-circuit model of this structure is shown in Fig. 1b [28], where  $L$  is the line inductance and  $C$  is the line capacitance in the region of the CSRR, and the CSRR is modelled by the resonant tank formed by  $L_c$  and  $C_c$ . Although there are well-known models that link the geometry of the structure to the circuit parameters (for instance, see [29] for the line and [28] for the CSRR), the line and the CSRR are not isolated but coupled, and this somehow affects the accuracy of the models to predict the

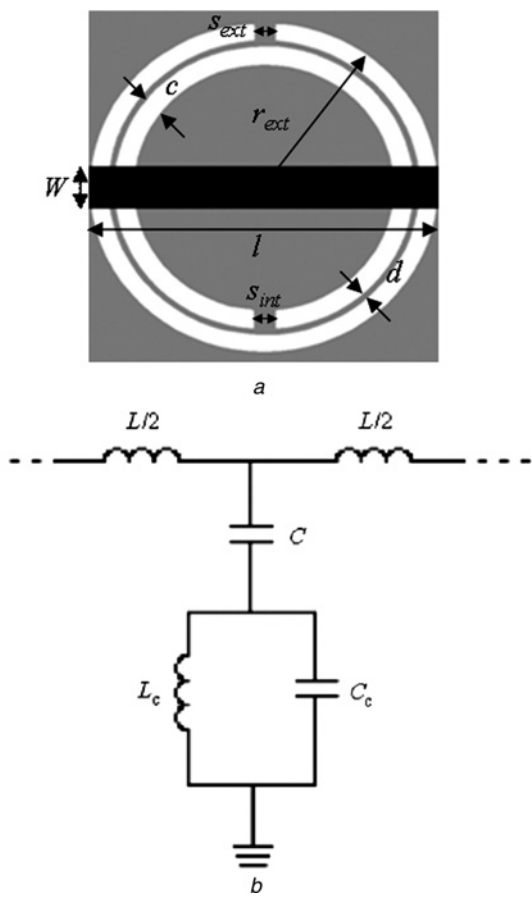


**Figure 1** Topology and T-circuit model

a Typical topology (unit cell) of a CSRR-loaded microstrip line  
b Equivalent T-circuit model  
Relevant geometrical parameters of the structure are indicated

circuit elements. To be more explicit, a metal (the conductor strip) on top of the CSRR affects the resonance frequency of the particle. Therefore it is expected that the predictions of the model [28] (which does not take into account the presence of a metal strip on the opposite substrate side) are different from the actual values of the resonator capacitance and inductance. In contrast, the line parameters are also affected by the presence of the ground plane slots of the CSRR. This means that we cannot use the existing models to directly determine the topology of CSRR-loaded lines from the circuit parameters of the electrical model of Fig. 1b. However, the determination of the circuit elements from a given topology (i.e. the inverse process) is straightforward. The parameter extraction method was published in [30], but it is reproduced here for coherence and completeness, as it will be used as part of the proposed ASM algorithm.

At the intercept of  $S_{11}$  with the unit resistance circle in the Smith chart, the shunt branch opens and hence we can determine the resonance frequency of the CSRR

$$f_o = \frac{1}{2\pi\sqrt{L_c C_c}} \quad (1)$$

as well as the value of the line inductance  $L$  (from the simulated series reactance at  $f_0$ ). To univocally determine the three circuit elements of the shunt branch, we need two additional conditions, apart from (1). One of them is the transmission zero frequency,  $f_z$ , which can be easily determined from the representation of the magnitude of  $S_{21}$  with frequency. The transmission zero obeys the expression

$$f_z = \frac{1}{2\pi\sqrt{L_c(C + C_c)}} \quad (2)$$

The third required condition can be

$$Z_s(j\omega_{-\pi/2}) = -Z_p(j\omega_{-\pi/2}) \quad (3)$$

where  $Z_s(j\omega)$  and  $Z_p(j\omega)$  are the series and shunt impedances of the T-circuit model of the structure, respectively, and  $\omega_{-\pi/2}$  is the angular frequency, where the phase of the transmission coefficient is  $\phi(S_{21}) = -\pi/2$ . Thus, from (1) to (3), we can determine the three reactive element values that contribute to the shunt impedance. The application of this parameter extraction method to a particular CSRR-loaded microstrip structure is reported in [30], with very good agreement between the circuit simulation, the electromagnetic (EM) simulation and the experiment (indeed, in [30], the method was applied to the measured frequency response of the structure, rather than to the EM simulation).

According to the previous paragraph, it is very clear that the determination of the circuit parameters from a certain given geometry is simple. The fact that the circuit and EM simulations are in very good agreement in the region of interests is indicative of the validity of the circuit model. However, the actual interest is in the inverse process, that is, the synthesis of layouts. Typically, from system specifications, we can easily determine the circuit elements of the model of Fig. 1b. The key point in the design is thus to find the geometry, providing an EM response as close as possible to the circuit simulation. In the past, this has been done with the help of the parameter extraction method and the experience of the designers. Alternatively, it can be done with the optimisation tools present in most commercial simulators, but this is very time-consuming and convergence problems typically arise. Therefore an accurate and fast synthesis method is of great interest. The purpose of this paper is to report an algorithm, based on ASM, for the automatic generation of the geometry of CSRR-loaded microstrip structures from a given set of circuit elements.

### 3 Synthesis based on ASM

#### 3.1 General formulation of ASM

Space mapping is a technique for EM optimisation originally proposed by Bandler *et al.* [25] in 1994, which makes proper use of two simulation spaces. In one space  $X_c$ , the variables

are linked to a coarse model, which is simple and computationally efficient, although not accurate, whereas in the other space  $X_f$ , the variables are linked to a fine model, typically more complex and CPU-intensive but significantly more accurate. In each space, we can define a vector containing different model parameters. Let us denote such vectors as  $x_f$  and  $x_c$  for the fine and coarse model parameters, respectively. Let us call  $R_f(x_f)$  the fine model response at  $x_f$  and  $R_c(x_c)$  the coarse model response at  $x_c$ . The key idea behind the space mapping optimisation is to generate an appropriate parameter transformation

$$x_c = P(x_f) \quad (4)$$

mapping the fine model parameter space to the coarse model parameter space such that

$$\|R_f(x_f) - R_c(x_c)\| \leq \varepsilon \quad (5)$$

in some predefined region,  $\|\cdot\|$  being a certain suitable norm and  $\varepsilon$  a small positive number.

If  $P$  is invertible, then the inverse transformation

$$x_f = P^{-1}(x_c^*) \quad (6)$$

is used to find the fine model solution, which is the image of the coarse model solution,  $x_c^*$ , giving the target response,  $R_c(x_c^*)$ . The determination of  $P$  follows an iterative process, which is the essence of the space mapping optimisation algorithm. Such iterative process was originally detailed in [25], and hence, it is not reproduced here. Nevertheless, we would like to mention that to determine the initial approximation of the mapping ( $P^{(1)}$ ), EM analysis of a pre-selected set of  $m$  base points in  $X_f$  (where  $m$  is the dimension of the vectors  $x_f$  and  $x_c$ ) is required. The base points are one reasonable candidate for the fine model solution, plus  $m - 1$  additional base points in its vicinity. Then the fine model responses are evaluated for each vector in  $X_f$ , and the corresponding vectors in  $X_c$  are obtained through parameter extraction. With both sets of vectors, we have  $m^2$  equations with  $m^2$  variables, which can be represented in the matrix form (4). The solution is the first transformation matrix  $P^{(1)}$ . By inverting this matrix, we can obtain a new vector in  $X_f$  from the coarse model solution

$$x_f = P^{(1)-1}(x_c^*) \quad (7)$$

Then the fine model response is obtained, and by extracting again the parameters of the coarse model, we have a new pair of vectors to update  $P(P^{(2)})$ . The process is iterated until convergence is achieved. The main penalty of this algorithm is that the EM analysis must be performed in  $m - 1$  additional points during the first iteration, and this makes the classical space mapping implementation rather inefficient [25].

As pointed out in [26], the efficiency of the previous method can be improved by introducing a quasi-Newton-type iteration. This aggressively exploits each fine model EM analysis with the result of a fast convergence. This new approach was called ASM [26], and it is the optimisation procedure used in this work. Essentially, the goal in ASM is to solve the following set of non-linear equations

$$\mathbf{f}(\mathbf{x}_f) = \mathbf{P}(\mathbf{x}_f) - \mathbf{x}_c^* = 0 \quad (8)$$

Let us assume that  $\mathbf{x}_f^{(j)}$  is the  $j$ th approximation to the solution of (8) and  $\mathbf{f}^{(j)}$  is the error function corresponding to  $\mathbf{f}(\mathbf{x}_f^{(j)})$ . The next vector of the iterative process  $\mathbf{x}_f^{(j+1)}$  is found by a quasi-Newton iteration according to

$$\mathbf{x}_f^{(j+1)} = \mathbf{x}_f^{(j)} + \mathbf{b}^{(j)} \quad (9)$$

where  $\mathbf{b}^{(j)}$  is given by

$$\mathbf{B}^{(j)} \mathbf{b}^{(j)} = -\mathbf{f}^{(j)} \quad (10)$$

and  $\mathbf{B}^{(j)}$  is an approach to the Broyden matrix [26]

$$\mathbf{B}^{(j+1)} = \mathbf{B}^{(j)} + \frac{\mathbf{f}^{(j+1)} \mathbf{b}^{(j)\text{T}}}{\mathbf{b}^{(j)\text{T}} \mathbf{b}^{(j)}} \quad (11)$$

which is also updated at each iterative step. In (11),  $\mathbf{f}^{(j+1)}$  is obtained by evaluating (8) using a certain parameter extraction method providing the coarse model parameters from the fine model parameters, and the superscript T stands for transpose (so that the numerator in the second term of the right-hand side of (11) is a matrix and the denominator a real number).

The implementation of the ASM algorithm is well reported in [26]. If the fine and coarse models involve the same space parameters, then the first vector in the fine space is typically set equal to the target vector in the coarse space, and the Broyden matrix is initialised by forcing it to be the identity matrix. However, this is not the case considered in the present paper. The next step is to discuss the specific procedure that we have followed to implement the ASM algorithm.

### 3.2 ASM applied to CSRR-loaded lines

Let us first establish the two model spaces and the variables involved in each of them. The coarse model  $X_c$  is the circuit model of the CSRR-loaded line, whose variables are those appearing in Fig. 1b. In contrast, the fine model  $X_f$  is the EM model, which allows us to obtain the frequency response of the structure from its geometry and substrate parameters (in the present paper, we have used the EM solver Agilent Momentum). In the EM model, we will consider that the substrate thickness  $b$  and dielectric constant  $\epsilon_r$ , as well as the metal layer parameters, are fixed. Specifically, in the present work,  $b = 1.27$  mm,  $\epsilon_r = 10.2$

(these parameters are those of the commercial Rogers RO3010 substrate) and both ohmic and dielectric losses have been excluded (in order to better check the capability of the algorithm to provide good solutions, as the circuit model does not include losses). Thus, the parameters of the EM space are those providing the topology of the structure. We will assume in this work that the CSRRs are round-shaped, but of course other topologies could have been considered (square-shaped, for instance). If we look at the structure of Fig. 1a, we need three parameters to fully specify CSRR dimensions. These are the external CSRR radius  $r_{\text{ext}}$ , the width of the slot rings  $c$  and the separation between them  $d$  (or another linear combination of the three mentioned parameters). Split dimensions are taken as  $s_{\text{ext}} = 0.07r_{\text{ext}}$  for the external ring and  $s_{\text{int}} = 0.07(r_{\text{ext}} - c - d)$  for the internal ring. This corresponds, approximately, to a gap aperture of  $4^\circ$  for each ring. Concerning the microstrip line (upper metal layer), its dimensions are specified by providing its length  $l$  and its width  $W$ . Hence, we need five geometrical parameters to fully determine the topology of the structure, whereas the circuit model only depends on four electrical parameters. In order to handle with the same number of parameters in both spaces, we will consider from now on that  $l = 2r_{\text{ext}}$ , so that the number of geometrical parameters of the EM model is reduced to 4. Other possibilities could have been considered, but the selected constraint must conceptually guarantee the layout implementation from the given circuit model parameters (of course, if the circuit parameters are too extreme – very high or very low – it might not be possible to generate the layout, even by considering the whole five variable parameters). The practical reason to consider  $l = 2r_{\text{ext}}$  is that the length  $l$  cannot be smaller than the CSRR external diameter (the ports of the structure must be accessed through lines not affected by the presence of the CSRR), and it can be only slightly larger than CSRR diameter (to avoid parasitic transmission line effects in the model of Fig. 1). Thus, the proposed constraint seems to be very reasonable, but not limitative at all.

Once the two space variables are clearly established, the next step is to determine the initial geometry  $\mathbf{x}_f^{(1)}$  from a given set of circuit parameters  $\mathbf{x}_c^*$  (whose electrical response is the target response of the EM model). To this end, we can make use of the well-known formulas linking the line geometry to the line parameters ( $L, C$ ) [29] and the model providing the CSRR inductance and capacitance [28] from its geometrical parameters. However, it has been verified from parameter extraction in different test structures that the circuit parameters depart significantly from the model predictions (this aspect has been discussed before). The reason is that the line affects the CSRR (the model reported in [28] is valid in the absence of metal layer in the side opposite to CSRR etching) and vice versa. In principle, this is not a problem, but if we determine the initial geometry from the analytical models, then  $L$  and  $C$  univocally determine  $l$  and  $W$ ; the external radius of the CSRR is thus  $l/2$  and  $c$  and  $d$  are univocally determined

from  $L_c$  and  $C_c$ . By proceeding in that way, we have experienced convergence problems, which are attributed to the fact that the initial geometry is rather different from the actual geometry providing the target circuit parameters (final solution in  $X_f$ ). Hence, we have proceeded as follows: from the resulting line impedance corresponding to  $L$  and  $C$ , we have determined, from standard formulas (and with the help of a transmission line calculator), the line width  $W$ , but not the line length. We have then set the ring slot width to a reasonable value ( $c = 0.25$  mm), taking into account that values of  $c$  much smaller than 0.2 mm are difficult to achieve in practice (because of technology limitations), and much larger than 0.3 mm are not convenient if we want to achieve electrically small designs. By forcing  $c$  to have a certain value,  $d$  and  $r_{ext}$  are univocally determined from  $C_c$  and  $L_c$ , and hence  $l$ , as  $l = 2r_{ext}$ . The reason is that once  $c$  is set to a certain value, the capacitance of the CSRR per unit length is determined and hence  $r_{ext}$ . Once  $r_{ext}$  is known,  $d$  results from the required value of  $L_c$ . Notice also that  $c$  is set to the value given above only for the determination of the initial geometry. After that,  $c$  is a variable.

From the initial geometry, we extract the circuit parameters, and hence, we have the error function (8) for the first iteration. The next step is the determination of the first approach to the Broyden matrix. To this end, we have slightly perturbed each geometrical parameter from the value obtained in the first layout, and we have extracted the circuit parameters corresponding to each geometry variation. The relative changes can be expressed in a matrix form as follows

$$\begin{pmatrix} \frac{\delta L}{\delta W} & \frac{\delta L}{\delta r_{ext}} & \frac{\delta L}{\delta c} & \frac{\delta L}{\delta d} \\ \frac{\delta C}{\delta W} & \frac{\delta C}{\delta r_{ext}} & \frac{\delta C}{\delta c} & \frac{\delta C}{\delta d} \\ \frac{\delta L_c}{\delta W} & \frac{\delta L_c}{\delta r_{ext}} & \frac{\delta L_c}{\delta c} & \frac{\delta L_c}{\delta d} \\ \frac{\delta C_c}{\delta W} & \frac{\delta C_c}{\delta r_{ext}} & \frac{\delta C_c}{\delta c} & \frac{\delta C_c}{\delta d} \end{pmatrix} \quad (12)$$

which corresponds to the initial Broyden matrix values. Once the Broyden matrix is known, the geometry of the following iteration can be derived from (9), and the process is iterated as explained earlier until convergence is obtained.

In practice, the iterative algorithm is controlled from the MATLAB commercial software, which acts as the core tool of the implemented ASM algorithm. There are three main building blocks in the MATLAB program: a module for the determination of the initial geometry of the structure (from the target circuit parameters), an EM solver (linked to the Agilent Momentum commercial software) and a module for parameter extraction. Concerning the module for the determination of the initial geometry, the analytical model for a microstrip structure [29] and the

CSRR model reported in [28] are used. The EM solver creates the topology of the strip line (in the upper metal level) and the topology of the CSRR (lower metal layer), from the geometrical parameters of the structure – a polar-to-Cartesian coordinate transformation is required for the generation of the CSRR geometry. Then, it is exported to the Agilent Momentum commercial software, where the EM simulation is performed. The results of this simulation (the  $S$ -parameters) are then imported back to MATLAB and processed by the parameter extraction module, which allows us to extract the circuit parameters. These are compared with the target parameters, and the error function is obtained. From this, the next geometry of the iterative process is inferred, following the update procedure described before.

## 4 Illustrative examples

To illustrate the capability of the proposed ASM-based synthesis technique to generate the layout of CSRR-based structures, we will consider two different case studies in the present section.

### 4.1 Example 1

In the first case considered, the target parameters in the circuit model are  $L^* = 5.08$  nH,  $C^* = 4.43$  pF,  $L_c^* = 2.98$  nH and  $C_c^* = 4.06$  pF (we assume that the circuit response with these parameters is the desired frequency response of the CSRR-loaded line). One important aspect, not discussed before, is the frequency range considered in the EM simulations. The circuit model of Fig. 1b is valid in a limited frequency range. However, as the error function for each iteration is obtained by comparing the extracted and the target circuit parameters rather than the target frequency response and the EM simulation, the considered frequency interval is not critical as long as it includes the frequencies of interests (namely, those necessary to extract the circuit parameters). These frequencies are the resonance frequency of the CSRR, given by (1), and other lower frequencies. Hence, the maximum considered frequency is set to  $f_{max} = 2f_o$ . From the target circuit parameters, we have inferred the first layout of the structure (depicted in Fig. 2a), following the procedure described in the previous section. Then, we have calculated the first Broyden matrix according to (12), and we have let the algorithm to evolve. The error function has been evaluated according to the following standard norm

$$\|f(x_f)\| = \sqrt{(L^* - L)^2 + (C^* - C)^2 + (L_c^* - L_c)^2 + (C_c^* - C_c)^2} \quad (13)$$

and we have forced the iterative algorithm to stop when the norm is less than 0.05, with the inductive values given in nH and the capacitances in pF. In the case considered, convergence has been achieved after 15 iterations. The

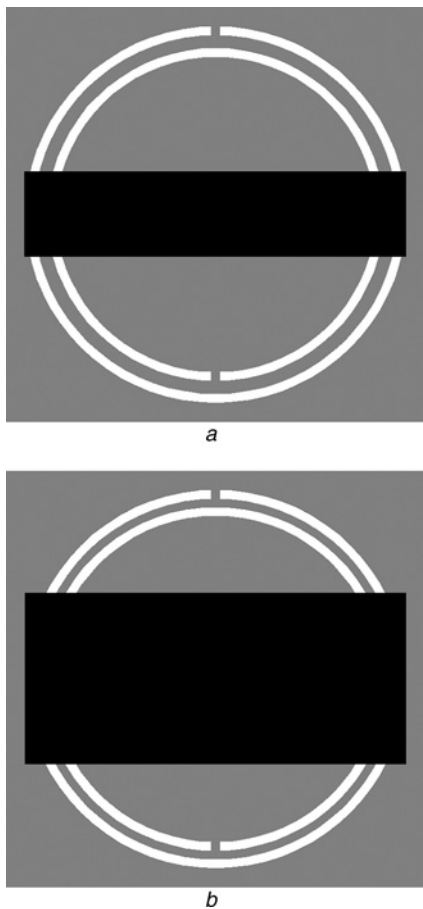


**Figure 2** Layouts of the structure of example 1

a Initial  
b Final

Initial layout dimensions are  $r_{\text{ext}} = 5.33 \text{ mm}$ ,  $d = 0.37 \text{ mm}$ ,  $W = 2.42 \text{ mm}$ ,  $c = 0.25 \text{ mm}$ ; the dimensions of the final layout are  $r_{\text{ext}} = 5.60 \text{ mm}$ ,  $d = 0.25 \text{ mm}$ ,  $W = 5.08 \text{ mm}$ ,  $c = 0.26 \text{ mm}$

target layout is depicted in Fig. 2b (see in the caption the geometrical parameters of the initial and final layouts). In Fig. 3, the target response (i.e. the circuit simulation by considering the target circuit parameters), the EM simulation of the layout of Fig. 2b and the EM simulation at iterations 3, 5 and 10 are depicted. The resulting circuit parameters after convergence ( $L = 5.09 \text{ nH}$ ,  $C = 4.45 \text{ pF}$ ,  $L_c = 2.96 \text{ nH}$  and  $C_c = 4.09 \text{ pF}$ ) are very close to the target parameters. Also, the EM simulation of the final layout is in very good agreement with the target circuit simulation, and it can be appreciated in Fig. 3 that the intermediate responses progressively evolve to the final response.

The target circuit parameters of this first example were chosen to be those inferred from parameter extraction performed in [30]. The geometry of the generated CSRR-loaded line (see caption of Fig. 2) is in very good agreement with the structure of [30]. Proceeding in this way, the algorithm implementation is fully validated.

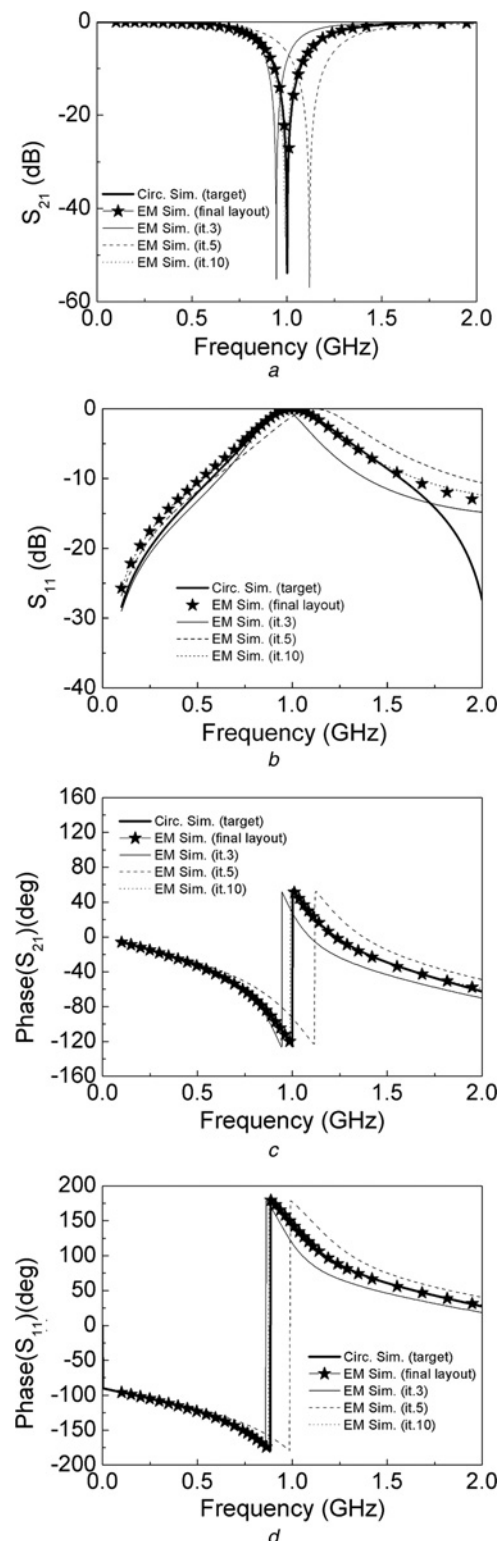


**Figure 3** Target frequency response for the structure of example 1 (obtained from circuit simulation of the model of Fig. 1 with the target parameters) and EM simulation at the indicated iteration steps and after convergence

a Insertion losses  
b Return losses  
c Phase of  $S_{21}$   
d Phase of  $S_{11}$

The number of EM simulations required to reach convergence has been 20

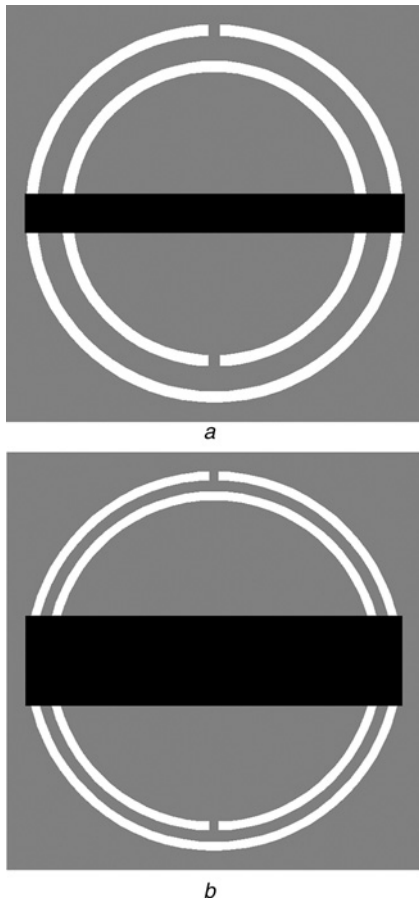


**Figure 4** Layouts of the structure of example 2

a Initial  
b Final

Initial layout dimensions are  $r_{\text{ext}} = 4.18 \text{ mm}$ ,  $d = 0.55 \text{ mm}$ ,  $W = 0.87 \text{ mm}$ ,  $c = 0.25$ ; the dimensions of the final layout are  $r_{\text{ext}} = 3.98 \text{ mm}$ ,  $d = 0.23 \text{ mm}$ ,  $W = 1.89 \text{ mm}$ ,  $c = 0.19 \text{ mm}$

## 4.2 Example 2

In the second example, the target circuit model parameters are  $L^* = 5.00 \text{ nH}$ ,  $C^* = 1.50 \text{ pF}$ ,  $L_c^* = 2.00 \text{ nH}$  and  $C_c^* = 3.00 \text{ pF}$ . In this case, convergence has been achieved after 16 iterations. The seeding layout and the final layout are both depicted in Fig. 4 (see in the caption the geometrical parameter values). The target response, the EM response after the last iteration and several intermediate responses are shown in Fig. 5. Again, the results are satisfactory with a very good agreement between the circuit simulation and the EM simulation after reaching convergence. However, a certain mismatch in the  $S_{11}$  parameter can be observed. Specifically, a reflection zero at 1 GHz is visible in the circuit simulation, not being present in the EM simulation of the resulting layout. Such reflection zero is due to the image impedance of the structure, which is exactly  $50 \Omega$  at 1 GHz for the circuit model with target parameters. The sensitivity of the reflection zero with regard to the circuit parameters is very high, and a small variation of these parameters may even cause the reflection zero to disappear. This also applies to

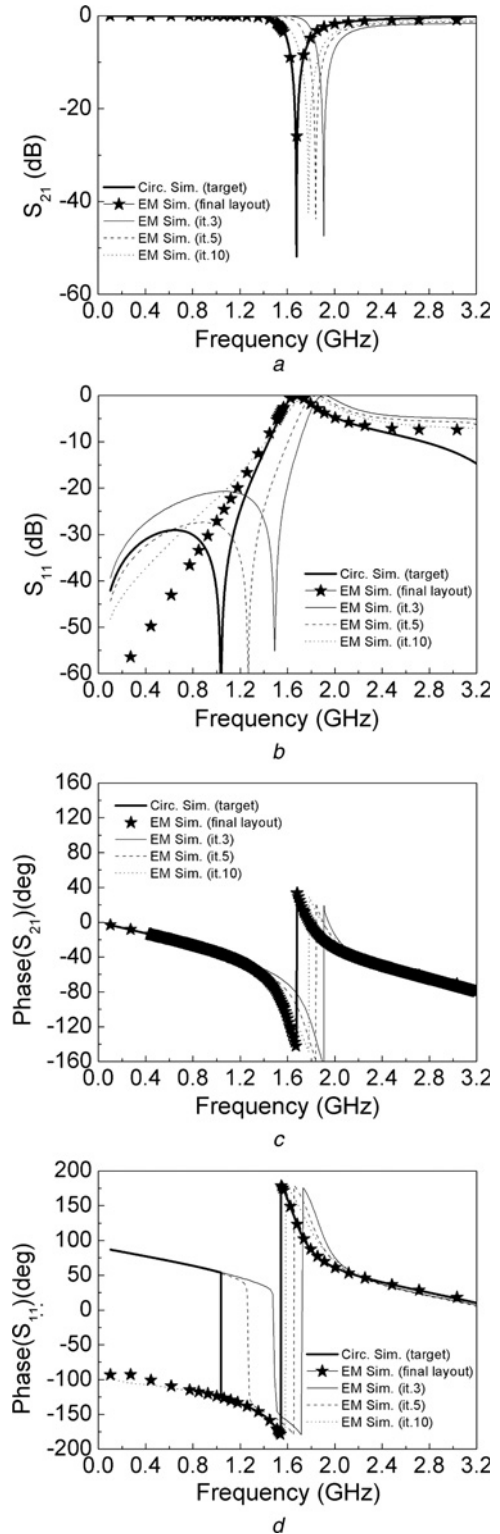


**Figure 5** Target frequency response for the structure of example 2 (obtained from circuit simulation of the model of Fig. 1 with the target parameters) and EM simulation at the indicated iteration steps and after convergence

a Insertion losses  
b Return losses  
c Phase of  $S_{21}$   
d Phase of  $S_{11}$

The number of EM simulations required to reach convergence has been 21

the geometry of the structure, and it is the reason for the mismatch in  $S_{11}$ . Nevertheless, this discrepancy in magnitude is not significant, and the agreement between the target response and the final EM response in the region of interest, i.e. in the vicinity of CSRR resonance, is excellent. In this example, the resulting circuit parameters after convergence ( $L = 5.01 \text{ nH}$ ,  $C = 1.50 \text{ pF}$ ,  $L_c = 1.98 \text{ nH}$  and  $C_c = 3.05 \text{ pF}$ ) are also very close to the target circuit parameters.

## 5 Conclusions

In conclusion, it has been demonstrated that the ASM technique is useful for the automatic generation of the layout of CSRR-loaded microstrip lines subjected to system specifications. From a certain set of circuit parameters (target parameters), which provide the target frequency response according to the circuit model of these lines, we are able to determine the topology (layout) of the structure providing the same EM response, without human intervention in the process. The implemented ASM optimisation algorithm, controlled from the MATLAB commercial software, contains a module for the determination of the initial geometry of the structure (from the target circuit parameters), an EM simulation solver (based on the Agilent Momentum commercial software) and a module for parameter extraction. These are the required building blocks for the implementation of the quasi-Newton-type iterative algorithm, in which ASM relies on. A relevant point of this paper has been the discussion for selecting the preferred four-element set of EM model parameters. The number of parameters in the circuit and EM model has been chosen to be the same in order to simplify the algorithm. In that way, the Broyden matrix is a square matrix, which is invertible. We have concluded that the most convenient geometrical parameters are the line width, the external radius of the CSRRs and the width and separation of the rings forming the CSRR, so that the line length has been set to twice the external CSRR radius. We have applied the implemented ASM algorithm to the synthesis of two CSRR-loaded microstrip line unit cells. In both cases, convergence has been achieved after few iterations, and the agreement between the target frequency responses and the EM simulation of the resulting structures has been found to be good. Work is in progress towards the modification of the technique for its application in more complex structures based on CSRRs and SRRs. Specifically, we have in mind to add a series gap to the CSRR structure in order to achieve a band-pass-type behaviour (with left-handed wave propagation).

## 6 Acknowledgments

This work has been supported by MEC (Spain) through the projects TEC2007-68013-C02 METAINNOVA and TEC2007-67630-C03 CABESERES and by MCI (Spain) through the project EMET CSD2008-00066 of the CONSOLIDER Ingenio 2010 Program. The authors especially thank Generalitat de Catalunya for funding

CIMITEC and for supporting GEMMA through the project 2009SGR-421. The Ministerio de Education (Spain) has given an FPU grant to J.S. with reference AP2008-04707.

## 7 References

- [1] ELEFTHERIADES G.V., BALMAIN K.G.: 'Negative-refraction metamaterials: fundamental principles and applications' (John Wiley & Sons Inc., New York, 2005)
- [2] CALOZ C., ITOH T.: 'Electromagnetic metamaterials: transmission line theory and microwave applications' (John Wiley & Sons Inc., New York, 2006)
- [3] MARQUÉS R., MARTÍN F., SOROLLA M.: 'Metamaterials with negative parameters: theory, design and microwave applications' (John Wiley & Sons Inc., New York, 2007)
- [4] IYER K., ELEFTHERIADES G.V.: 'Negative refractive index metamaterials supporting 2-D waves'. IEEE-MTT Int. Microwave Symp., Seattle, WA, June 2002, vol. 2, pp. 1067–1070
- [5] OLINER A.: 'A periodic-structure negative-refractive-index medium without resonant elements'. URSI Dig. IEEE-AP-S USNC/URSI National Radio Science Meeting, San Antonio, TX, June 2002, p. 41
- [6] CALOZ C., ITOH T.: 'Application of the transmission line theory of left-handed (LH) materials to the realization of a microstrip LH transmission line'. Proc. IEEE-AP-S USNC/URSI National Radio Science Meeting, San Antonio, TX, June 2002, vol. 2, pp. 412–415
- [7] PENDRY J.B., HOLDEN A.J., ROBBINS D.J., STEWART W.J.: 'Magnetism from conductors and enhanced nonlinear phenomena', *IEEE Trans. Microw. Theory Tech.*, 1999, **47**, pp. 2075–2084
- [8] MARTÍN F., FALCONE F., BONACHE J., MARQUÉS R., SOROLLA M.: 'Split ring resonator based left handed coplanar waveguide', *Appl. Phys. Lett.*, 2003, **83**, pp. 4652–4654
- [9] FALCONE T., LOPETEGI BAENA J.D., MARQUÉS R., MARTÍN F., SOROLLA M.: 'Effective negative- $\epsilon$  stop-band microstrip lines based on complementary split ring resonators', *IEEE Microw. Wirel. Comp. Lett.*, 2004, **14**, pp. 280–282
- [10] FALCONE F., LOPETEGI T., LASO M.A.G., ETAL.: 'Babinet principle applied to the design of metasurfaces and metamaterials', *Phys. Rev. Lett.*, 2004, **93**, pp. 197401-1–197401-4
- [11] CALOZ C., ITOH T.: 'Novel microwave devices and structures based on the transmission line approach of metamaterials'. IEEE-MTT Int. Microwave Symp., Philadelphia, PA, June 2003, vol. 1, pp. 195–198

- [12] GIL M., BONACHE J., SELGA J., GARCÍA-GARCÍA J., MARTÍN F.: 'Broadband resonant type metamaterial transmission lines', *IEEE Microw. Wirel. Comp. Lett.*, 2007, **17**, pp. 97–99
- [13] GIL M., BONACHE J., GARCÍA-GARCÍA J., MARTEL J., MARTÍN F.: 'Composite right/left handed (CRLH) metamaterial transmission lines based on complementary split rings resonators (CSRRs) and their applications to very wide band and compact filter design', *IEEE Trans. Microw. Theory Tech.*, 2007, **55**, pp. 1296–1304
- [14] MONDAL P., MANDAL M.K., CHAKRABARTY A., SANYAL S.: 'Compact bandpass filters with wide controllable fractional bandwidth', *IEEE Microw. Wirel. Comp. Lett.*, 2006, **16**, pp. 540–542
- [15] BONACHE J., FALCONE F., BAENA J.D., ET AL.: 'Application of complementary split rings resonators to the design of compact narrow band pass structure in microstrip technology', *Microw. Opt. Technol. Lett.*, 2005, **46**, pp. 508–512
- [16] BONACHE J., GIL I., GARCÍA-GARCÍA J., MARTÍN F.: 'Novel microstrip band pass filters based on complementary split rings resonators', *IEEE Trans. Microw. Theory Tech.*, 2006, **54**, pp. 265–271
- [17] MONDAL P., MANDAL M.K., CHAKRABARTY A., SANYAL S.: 'Compact bandpass filters with wide controllable fractional bandwidth', *IEEE Microw. Wirel. Comp. Lett.*, 2006, **16**, pp. 540–542
- [18] WU H.-W., SU Y.-K., WENG M.-H., HUNG C.-Y.: 'A compact narrow-band microstrip band pass filter with a complementary split ring resonator', *Microw. Opt. Technol. Lett.*, 2006, **48**, pp. 2103–2106
- [19] BONACHE J., POSADA G., GARCHON G., DE RAEDT W., MARTÍN F.: 'Compact ( $<0.5 \text{ mm}^2$ ) K-band metamaterial band pass filter in MCM-D technology', *Electron. Lett.*, 2007, **43**, pp. 45–46
- [20] BORJA A.L., CARBONELL J., BORIA V.E., LIPPENS D.: 'Highly selective left-handed transmission line loaded with split ring resonators and wires', *Appl. Phys. Lett.*, 2009, **94**, pp. 143503-1–143503-3
- [21] ROGLÁ L.J., CARBONELL J., BORIA V.E.: 'Study of equivalent circuits for open-ring and split-ring resonators in coplanar waveguide technology'. *IET Proc. Microw. Antennas Propag. (Special Issue on Metamaterials LHM)*, 2007, **1**, pp. 170–176
- [22] MARTÍN F., FALCONE F., BONACHE J., LOPETEGI T., MARQUÉS R., SOROLLA M.: 'Miniaturized CPW stop band filters based on multiple tuned split ring resonators', *IEEE Microw. Wirel. Comp. Lett.*, 2003, **13**, pp. 511–513
- [23] GARCÍA-GARCÍA J., MARTÍN F., FALCONE F., ET AL.: 'Microwave filters with improved stop band based on sub-wavelength resonators', *IEEE Trans. Microw. Theory Tech.*, 2005, **53**, pp. 1997–2006
- [24] CARBONELL J., BORJA A.L., BORIA V.E., LIPPENS D.: 'Duality and superposition in split-ring-resonator-loaded planar transmission lines', *IEEE Antennas Wirel. Propag. Lett.*, 2009, **8**, pp. 886–889
- [25] BANDLER J.W., BIERNACKI R.M., CHEN S.H., GROBELNY P.A., HEMMERS R.H.: 'Space mapping technique for electromagnetic optimization', *IEEE Trans. Microw. Theory Tech.*, 1994, **42**, pp. 2536–2544
- [26] BANDLER J.W., BIERNACKI R.M., CHEN S.H., HEMMERS R.H., MADSEN K.: 'Electromagnetic optimization exploiting aggressive space mapping', *IEEE Trans. Microw. Theory Tech.*, 1995, **43**, pp. 2874–2882
- [27] ROGLÁ L.J., RAYAS-SÁNCHEZ J.E., BORIA V.E., CARBONELL V.E.: 'EM-based space mapping optimization of left-handed coplanar waveguide filters with split ring resonators'. IEEE-MTT Int. Microwave Symp., Honolulu, Hawaii, June 2007, pp. 1241–1244
- [28] BAENA J.D., BONACHE J., MARTÍN F., ET AL.: 'Equivalent circuit models for split ring resonators and complementary split rings resonators coupled to planar transmission lines', *IEEE Trans. Microw. Theory Tech.*, 2005, **53**, pp. 1451–1461
- [29] POZAR D.M.: 'Microwave engineering' (Addison Wesley, 1990)
- [30] BONACHE J., GIL M., GIL I., GARCIA-GARCÍA J., MARTÍN F.: 'On the electrical characteristics of complementary metamaterial resonators', *IEEE Microw. Wirel. Comp. Lett.*, 2006, **16**, pp. 543–545